AD-A099 829 NAVAL SURFACE WEAPONS CENTER DAHLGREN VA F/G 17/7
FORMULATION FOR THE NAVSTAR GEODETIC RECEIVER SYSTEM (NGRS).(U)
MAR 81 B R HERMANN
UNCLASSIFIED NSWC/TR-80-348 NL

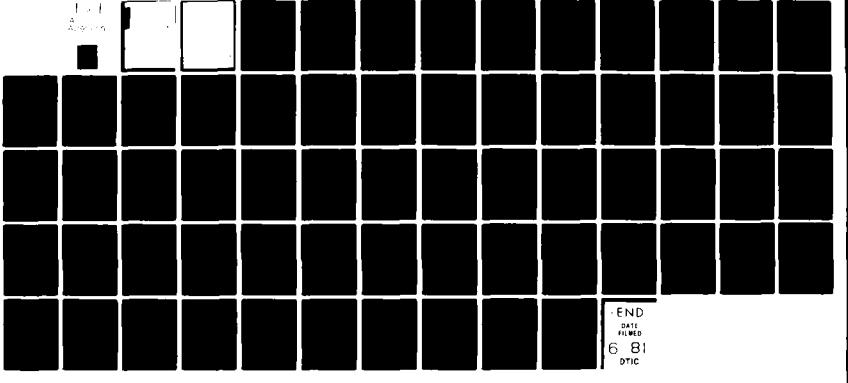

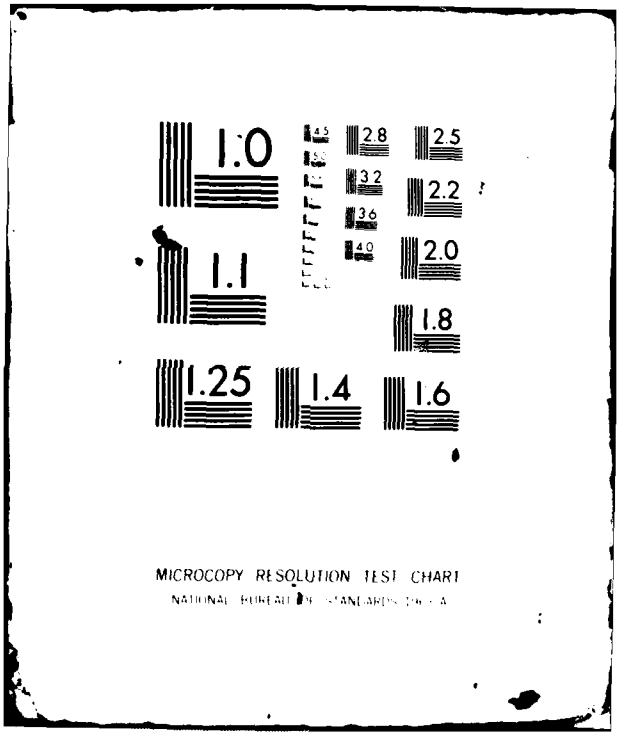
1.0
1.1
1.25
1.4
1.6
1.8
2.0
2.2
2.5
2.8
3.2
3.6
4.0
MICROCOPY RESOLUTION TEST CHART

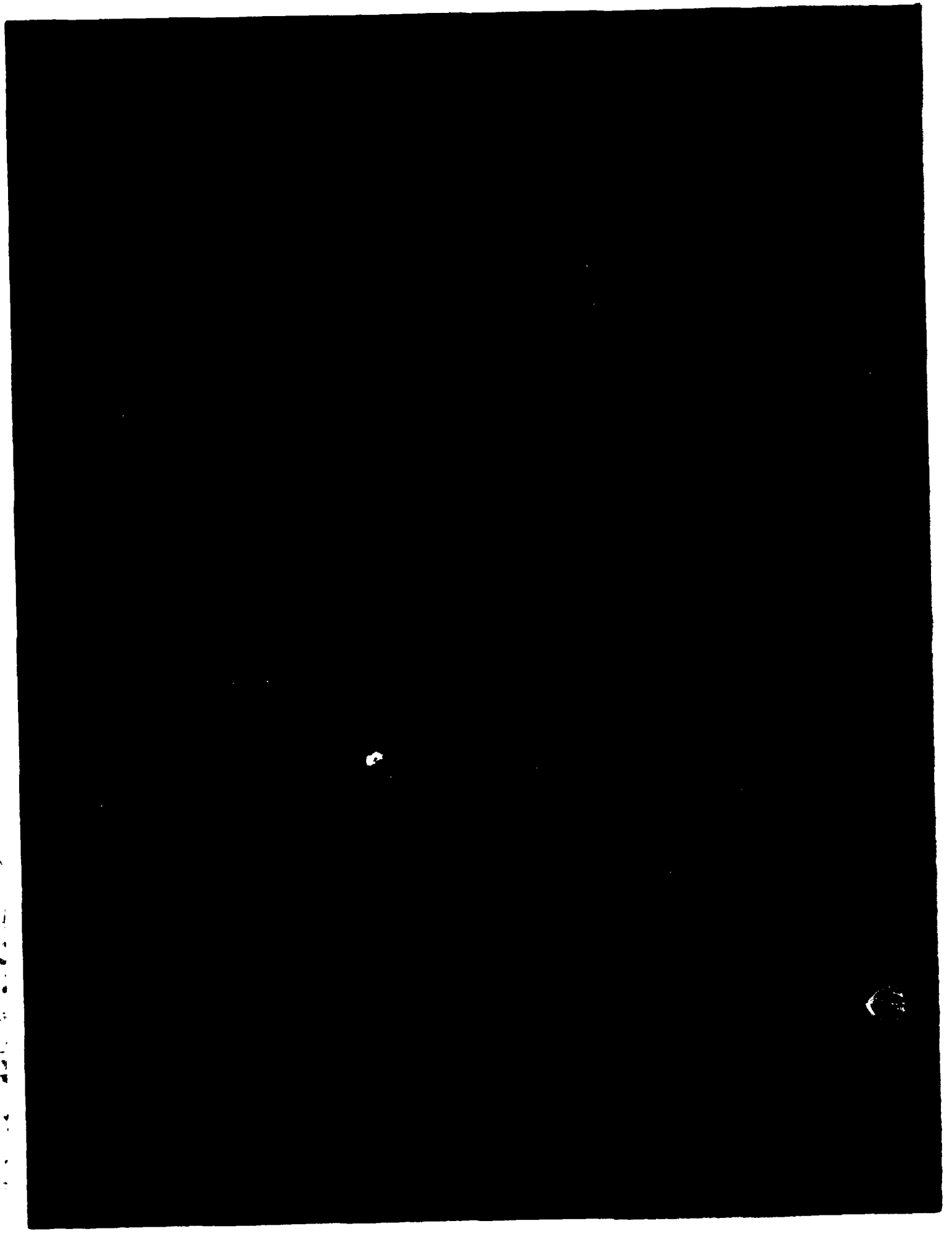

UNCLASSIFIED

SECURITY CLASSIFICATION OF THIS PAGE (When Data Entered)

REPORT DOCUMENTATION PAGE	READ INSTRUCTIONS BEFORE COMPLETING FORM
1. REPORT NUMBER: NSWC/TR-80-348	2. GOVT ACCESSION NO.: AD-A099 829	3. RECIPIENT'S CATALOG NUMBER
4. TITLE (and Subtitle): Formulation for the NAVSTAR Geodetic Receiver System (NGRS)	5. TYPE OF REPORT & PERIOD COVERED: Final Rept.
	6. PERFORMING ORG. REPORT NUMBER
7. AUTHOR(s): Bruce R. Hermann	8. CONTRACT OR GRANT NUMBER(s)
9. PERFORMING ORGANIZATION NAME AND ADDRESS: Naval Surface Weapons Center (K13), Dahlgren, VA 22448	10. PROGRAM ELEMENT, PROJECT, TASK AREA & WORK UNIT NUMBERS: 65 (12) 64
11. CONTROLLING OFFICE NAME AND ADDRESS: Headquarters, Defense Mapping Agency, Washington, D.C. 20360	12. REPORT DATE: Mar[illegible]81
	13. NUMBER OF PAGES: 68
14. MONITORING AGENCY NAME & ADDRESS(if different from Controlling Office)	15. SECURITY CLASS. (of this report): UNCLASSIFIED
	15a. DECLASSIFICATION/DOWNGRADING SCHEDULE

16. DISTRIBUTION STATEMENT (of this Report)

Approved for public release; distribution unlimited.

17. DISTRIBUTION STATEMENT (of the abstract entered in Block 20, if different from Report)

18. SUPPLEMENTARY NOTES

19. KEY WORDS (Continue on reverse side if necessary and identify by block number)

NAVSTAR Global Positioning System (GPS)
NAVSTAR Geodetic Receiver System (NGRS)
Geodetic Point Positioning
Doppler Frequency (Velocity)
Doppler Rate (Acceleration)

20. ABSTRACT (Continue on reverse side if necessary and identify by block number)

The NAVSTAR Global Positioning System (GPS) can be used for geodetic applications. The NAVSTAR Geodetic Receiver System (NGRS) has been developed to demonstrate this capability. A brief description of the NGRS hardware is presented along with the formulation that converts the observations of satellite Doppler frequency to range differences. The sensitivity of the range differences to random error sources is also discussed.

DD FORM 1 JAN 73 1473 EDITION OF 1 NOV 65 IS OBSOLETE
S/N 0102-LF-014-6601

UNCLASSIFIED

SECURITY CLASSIFICATION OF THIS PAGE (When Data Entered)

FOREWORD

The development of the NAVSTAR Geodetic Receiver System (NGRS) was funded by the Defense Mapping Agency as a test bed to demonstrate the capability of using satellite Doppler data to achieve high accuracy geodetic point positioning. The receiver was designed by Stanford Telecommunications, Incorporated, under contract to the Naval Surface Weapons Center (NSWC). The supporting hardware definition and the system microprocessor controller software were proposed and implemented at NSWC by the Electronics Systems Department, Advanced Projects Division. Technical and administrative assistance was received from the sponsor through the Defense Mapping Agency Hydrographic/Topographic Center in Washington, D.C.

This report has been reviewed by R. W. Hill, Head, Space Flight Sciences Branch, R. J. Anderle, Research Associate, and D. R. Brown, Jr., Head, Space and Surface Systems Division.

Released by:

R. T. RYLAND, Head
Strategic Systems Department

ACKNOWLEDGEMENTS

The author wishes to take this opportunity to acknowledge those who have had a role in the development of the NGRS. At NSWC, Mr. Richard Anderle, Research Associate, and Mr. Robert Hill, Head, Space Flight Sciences Branch, provided both administrative and technical support. Technical assistance was also provided by Mr. William Birmingham, Ms. Dee Batayte and Ms. Louise Gordon provided the programming support, and the author was assisted in the data reduction by Mr. Patrick Hoffman, Mr. Stanly Meyerhoff, and by Ms. D. Jeannie Haynie.

In the Electronics Systems Department, Mr. Theodore Saffos was responsible for the system hardware design and maintenance while supervising the development of the microprocessor system controller software. This software development was accomplished by Mr. Ralph Dickerson, Mr. Glen Bowen, and Mr. Eric Morgan.

Project direction, planning, and advice were offered by the Defence Mapping Agency through Mr. Benjamin Roth at SAMSO and Mr. Henry Heuerman at the Hydrographic/Topographic Center. Final authority rested with Dr. Charles Martin at Headquarters.

CONTENTS

FIGURES

TABLES

INTRODUCTION

The Astronautics and Geodesy Division in conjunction with the Advanced Projects Division of NSWC, with sponsorship by the Defense Mapping Agency, have developed a receiving system that allows the NAVSTAR Global Positioning System (GPS) to be used for geodetic point positioning. Previous experience with the Navy Navigation Satellite System has shown that observations of Doppler frequency from many satellite passes can be used to obtain positions at the receiving site with an error of only a few meters. It was hoped that similar techniques applied to the GPS constellation would allow even better results to be realized. It was to demonstrate this potential that the NGRS was developed.

SYSTEM DEFINITION

The heart of the NGRS is the GPS receiver, which was developed by the Stanford Telecommunications, Incorporated, under contract to NSWC. The receiver was delivered in September 1978. Integration of the receiver and the other equipment that comprise the NGRS progressed through the end of 1978. First data were processed in January 1979, and the system was declared operational at the end of that month. The truck containing the NGRS was driven to Yuma Proving Ground in early February for the initial tests alongside the Mobile Test Van, which contained a Magnavox "X-set" configured for static real-time positioning. The NGRS remained at the Yuma site until day 80 of 1979.

Figure 1 shows a block diagram of the NGRS, and a list of the equipment is given in Table 1. A description of the satellites and the signal structure is described in a special issue of the *Journal of the Institute of Navigation*[1]. Each satellite transmits on two L band frequencies: L_1 = 1575.42 MHz and L_2 = 1227.6 MHz. The bandwidth of the signals is about 20 MHz and consists of a carrier biphase modulated by two pseudo-random sequences having frequencies of 1.023 MHz (C/A) and 10.23 MHz (P). A data bit stream of frequency 50 Hz is added to each of the pseudo-random sequences. A replica of the C/A and P code is generated in the receiver and correlated with the incoming signal. The replica is shifted in time until a correlation peak is obtained. If this correlation peak is maintained, the local code is then locked to the incoming code from the satellite. The dependence of this correlation peak on bandwidth is described in Appendix A.

The pseudo-range measurement is obtained by recording the time interval between the local time epoch and the same epoch received from the satellite. This measurement consists of two parts: the propagation delay and the time offset between the local and satellite clocks. Figure 2 shows this relationship.

The analog Doppler signal derived from the reconstructed carrier in the receiver is used to obtain Doppler counts on both L_1 and L_2. The time interval over which the count is made is determined by the local clock and is nominally 60-s duration. A continuous running counter is strobed at the end of the interval to provide the integer count. The time from the end of the interval until the

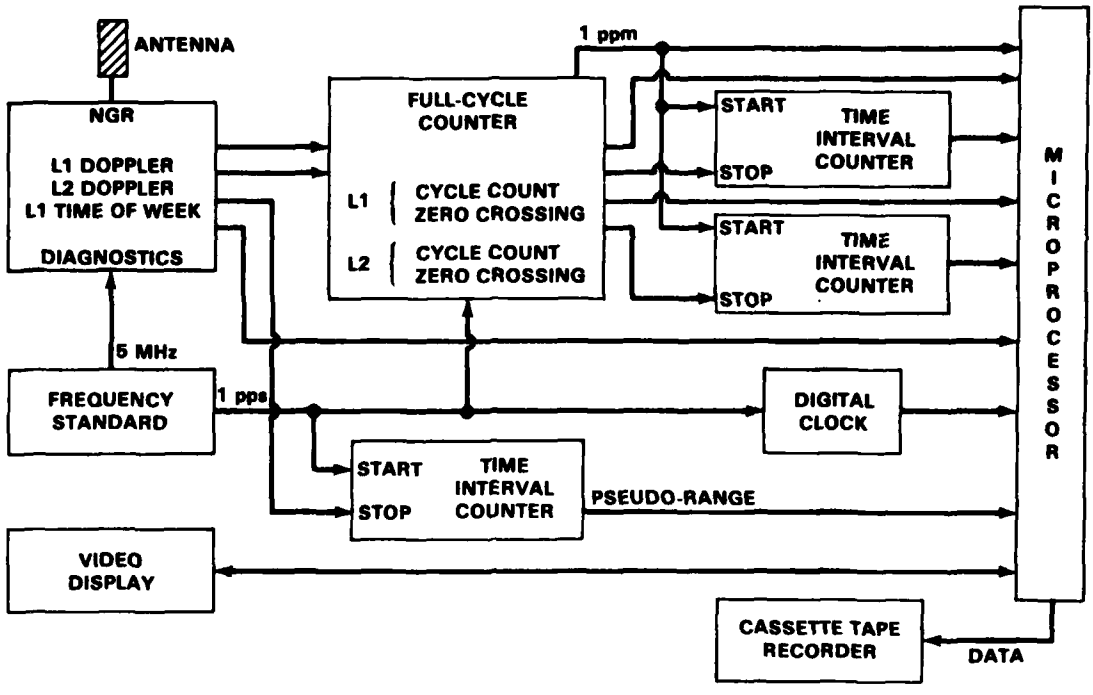

Figure 1. NGRS Block Diagram

Table 1. NGRS Components

Microprocessor	INTEL 80/10
Frequency Standards	HP 5061A
	HP 5062C
NAVSTAR Receiver	STI 5007
Time Interval Counters	HP 5328A
Digital Clock	HP 59309A
Full-Cycle Counter	NSWC
Video Display	BEEHIVE
L Band Antenna	CHU CA3207
Tape Recorder	DICOM 374
Test Transmitter	STI 5001A

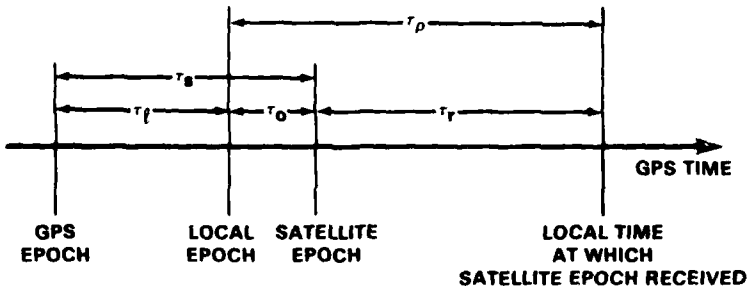

τ_r = PROPAGATION DELAY
τ_o = EPOCH OFFSET (SATELLITE - LOCAL)
τ_ρ = OBSERVATION OF PSEUDO-RANGE = $\tau_o + \tau_r$
τ_ℓ = EPOCH OFFSET (LOCAL - GPS)
τ_s = EPOCH OFFSET (SATELLITE - GPS) = $\tau_o + \tau_\ell$
A VALUE FOR τ_s IS FOUND IN THE SATELLITE DATA MESSAGE

Figure 2. Relationship Between the Time Systems and Pseudo Range

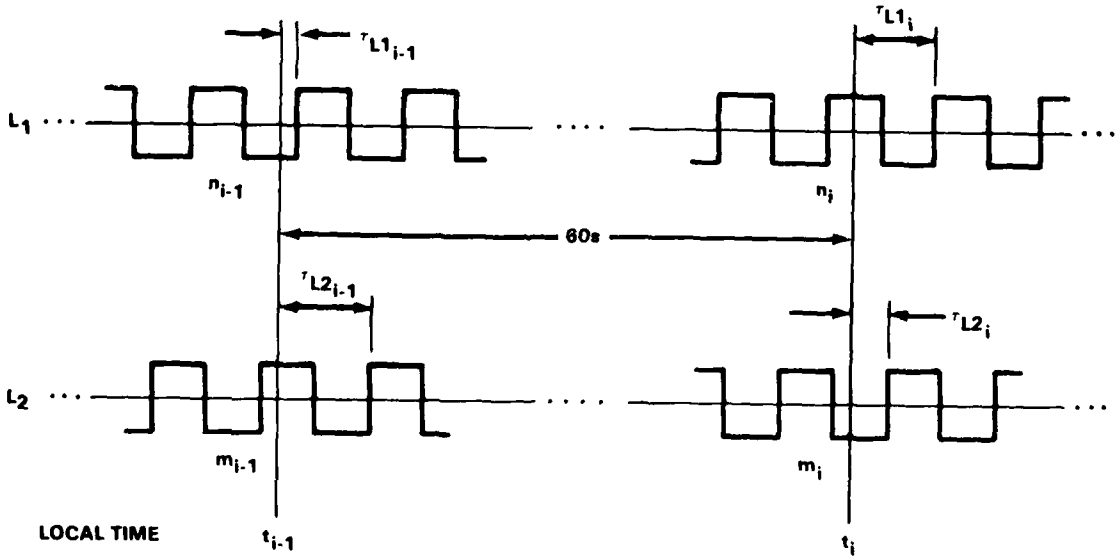

n AND m = THE ACCUMULATED COUNTS AT EACH LOCAL 60-s EPOCH

τ_{L1} AND τ_{L2} TIMES FROM THE LOCAL 60-s EPOCH TO THE NEXT POSITIVE GOING ZERO CROSSINGS

ZERO DOPPLER FREQUENCY = 28750 Hz

Figure 3. Measurements That Comprise the Doppler Observations

next positive zero crossing of the analog Doppler signal is also recorded. This allows a precise measurement of the true time interval to be made. A pictorial description of the process is shown in Figure 3.

The system operation is controlled by a microprocessor. To begin observing, the operator is asked to key in the options he wishes to use for the current session. Each response is displayed on the video terminal and sets flags in the controlling program. After a cassette tape is loaded into the tape drive, the system is ready to begin observations. A search is initiated for the first satellite using the Doppler estimate, which has been entered by the operator.

Two methods of operation are available: *local* and *remote*. In the *local* mode, the operator loads the acquisition information directly into the receiver via the front panel switches. This information consists of the satellite code identification number, the expected Doppler frequency with a tolerance of ± 500 Hz, and the differential ionospheric delay between the L_1 and L_2 channels. Acquisition of different satellites is made by entering new information when desired. The *remote* mode offers the option of entering a list of acquisition information and start times into the microprocessor via the the keyboard. The computer will then operate the receiver remotely, sending the new acquisition information at the preset times.

When the receiver has acquired the first satellite, pseudo-range measurements obtained from the time-interval counter are sent to the microprocessor each 6s. At the end of a minute, as determined by the local clock, the two Doppler counts and the two fractional counts are sent to the microprocessor. All the data accumulated during that minute are then recorded on the tape recorder. The system continues tracking in this 1-minute cycle until the satellite goes out of view, or the time arrives to search for a different satellite. The tape holds about 12 hr of continuous observations, and it can switch to a second drive when the first is full. The data from these cassettes are transferred to a nine-track tape and are then preprocessed. The preprocessed data are kept on disk packs for further processing as desired.

TIME CORRECTIONS

Time corrections are necessary so that the Doppler observations and the satellite reference trajectory are referred to the same time system. For our purposes, *time* is kept at the Master Control Station (MCS) at Vandenburg Air Force Base. This is GPS time and is allowed to follow its own course; that is, it is not corrected for the variations in the earth's rotation as is Universal Time.

Each GPS satellite has an independent frequency standard that must be corrected to GPS time. The corrections for each satellite are predicted by the MCS and uploaded. Each satellite, in turn, transmits these predicted corrections to its apparent time in its navigation message. The user must

then apply these corrections when he uses the data. In this way, all the data can be converted to a common time system.

In the NGRS, the single frequency (L_1) pseudo-range measurement is used to relate the local time to GPS time (Appendix B). The pseudo-range observation gets its name because it is just a *time-of-flight* range measurement treated as if the clocks on both ends were synchronized. In reality they are not synchronized; and so the measurement is not a true range, but includes the clock errors plus propagation effects. Figure 2 illustrates the measurement. Epoch is an arbitrary instant at which each clock registers the same numerical time. The observable is τ_ρ and is time tagged by the satellite epoch. However, the satellite epoch is offset from GPS time by τ_s (note that τ_s, as well as τ_t and τ_0, are not constant but vary with time). The navigation message from each GPS satellite gives the predicted values for τ_s as a function of GPS time. Thus, the true time (GPS time) tag for the observation is the satellite epoch time minus τ_s. This is the correction that needs to be made to the pseudo-range time tags to indicate the *true* time of transmission. With the use of the τ_ρ observations, the local clock offset τ_0 can be obtained by subtracting out the propagation delay τ_r. To calculate τ_r, the satellite position and the receiver position are needed. However, extreme position accuracy is not necessary because the relative velocity is much less than the propagation velocity.

If a worst-case relative velocity of 1000 m/s is assumed, the slant range changes by only 0.001 m in 1 μs. Light travels 300 m in 1 μs. Therefore, a position error of 300 m in the slant range would produce only 1-μs error in the value of τ_0. Microsecond accuracy in τ_0 is adaquate for this purpose. With τ_0 known, the local epoch can also be converted to GPS time. If t_l is the local time, the corresponding epoch converted to GPS would be t_l^*

where

$$t_l^* = t_l + \tau_s - \tau_0$$

In this equation, the senses in Figure 2 are used to determine the signs.

DOPPLER OBSERVATIONS

The Doppler observation consists of two measurements: the Doppler count is an integer that represents the accumulated number of Doppler cycles and is recorded at a regular interval T; and the time interval measurement is equivalent to a fractional cycle count. The interval measured is between each T epoch and the next positive going zero crossing of the analog Doppler signal. Both of these measurements are illustrated in Figure 3.

The signal that is counted is the difference between an offset frequency f_0 and the true Doppler f_d. Since f_0 = 28750 Hz, a count of zero Doppler would register 1,725,000 counts. The fractional count is combined with the integer count in the following manner. Referring to Figure 3, the time interval that represents the integer count is $T + \tau_{r-1} - \tau_r$. Therefore, the average frequency is $m \div (T + \tau_{r-1} - \tau_r)$ Hz. From the average frequency, the approximate number of counts in the interval T can be determined. This count, m_1, is

$$m_T = m + (\tau_{i-1} - \tau_i) \frac{m}{T + \tau_{i-1} - \tau_i}$$

The error introduced into m_T by using the average frequency is discussed in Appendix C.

The Doppler data consist of two simultaneous observations: one from L_1 and the other from L_2. These two frequencies will be refracted differently by the ionosphere because it is a dispersive medium. Solution of the resulting simultaneous equations allows a correction term to be evaluated, and substitution of this term into either of the original two equations will produce a corrected observation. The mechanics of this process will be developed in the sections that follow.

CLOCK MODEL

The clock model used in this development will be expressed as a phase function $\Phi(t)$.

$$\Phi(t) = \phi + 2\pi(\nu_0 + \nu(t))\, t + \eta(t) \tag{1}$$

where

$\Phi(t)$ = total phase accumulated since $t = 0$
ϕ = phase at $t = 0$; i.e., $\Phi(0) = \phi$
ν_0 = nominal oscillator frequency (constant)
$\nu(t)$ = deterministic frequency variation
$\eta(t)$ = random phase noise term

This form of the phase will represent both the local standard reference as well as the satellite reference.

The instantaneous frequency is $\dot{\Phi}(t)$

where

$$\dot{\Phi}(t) = 2\pi(\nu_0 + \nu(t)) + 2\pi\dot{\nu}(t)t + \dot{\eta}(t) \tag{2}$$

and at $t = 0$,

$$\Phi(0) = 2\pi(\nu_0 + \nu(0)) + \dot{\eta}(0)$$

The argument t will represent GPS time as kept by the MCS. All other clocks will have offset and rate differences when compared with the reference standard. A clock keeping perfect GPS time can be represented by a phase function of the following form:

$$\Phi_{GPS}(t) \quad 2\pi\nu_0 t \tag{3}$$

where ν_0 is a known invariant constant. Time is kept by keeping track of the phase $\Phi_{GPS}(t)$. A time interval would be represented by the difference of two phases at different instants.

$$t_2 - t_1 = \frac{1}{2\pi\nu_0} [\Phi_{GPS}(t_2) - \Phi_{GPS}(t_1)] \text{ seconds}$$

With the clock model defined as above, let the satellite clock be represented by

$$\Phi_s(t) = \phi_s + 2\pi(\nu_{0s} + \nu_s(t))\, t + \eta_s(t) \tag{4}$$

and the local clock by

$$\Phi_L(t) = \phi_L + 2\pi(\nu_{0L} + \nu_L(t))\, t + \eta_L(t)$$

DOPPLER SIGNAL MODEL

The signals recovered will be the transmitted signals perturbed by the ionosphere (troposphere and relativity effects will be ignored in this development). The ionosphere will be introduced as a time delay similar to the geometric propagation time. Let the total propagation delay be represented by τ_ρ

where

$$\tau_\rho = \frac{1}{c} (r + I) \text{ and } r(t) = \text{slant range from the satellite to receiver}$$

The second term, $I(t)$, is the ionospheric delay.

Signals transmitted at t_T are received at a later time $t_T + \tau_\rho$, or conversely the signals currently received were transmitted earlier at $t_R - \tau_\rho$. Before transmission, Equation 4 was multiplied by a constant q_1 for broadcast on L_1. Similarly, Equation 4 was multiplied by q_2 for broadcast on L_2. The received signals are represented by Equations 6a and 6b.

$$\Phi_{s1}(t_R - \tau_\rho) = q_1[\phi_s + 2\pi(\nu_{0s} + \nu_s)(t_R - \tau_\rho) + \eta_s(t_R - \tau_\rho)] \tag{6a}$$

$$\Phi_{s2}(t_R - \tau_\rho) = q_2[\phi_s + 2\pi(\nu_{0s} + \nu_s)(t_R - \tau_\rho) + \eta_s(t_R - \tau_\rho)] \tag{6b}$$

In the receiver, two similar signals are derived from the local clocks; these are represented by Equations 7a and 7b.

$$\Phi_{L1}(t_R) = q_1[\phi_R + 2\pi(\nu_{0L} + \nu_L)\, t_R + \eta_L(t_R)] \tag{7a}$$

$$\Phi_{L2}(t_R) = q_2[\phi_R + 2\pi(\nu_{0L} + \nu_L)\, t_R + \eta_L(t_R)] \tag{7b}$$

The receiver mixes the locally generated signals with those received and derives an intermediate frequency which is then processed. This intermediate frequency phase function will be written as the difference between Equations 6 and 7:

$$\Phi_{F1}(t_R) = \Phi_{s1}(t_R - \tau_\rho) - \Phi_{L1}(t_R)$$

$$= q_1\phi_s - \varrho_1\phi_R + 2\pi[q_1(\nu_{0s} + \nu_s)(t_R\,\tau_\rho) - \varrho_1(\nu_{0L} + \nu_L)t_R]$$

$$+ q_1\eta_s(t_R - \tau_\rho) - \varrho_1\eta_L(t_R) \tag{8a}$$

$$\Phi_{F2}(t_R) = \Phi_{s2}(t_R - \tau_\rho) - \Phi_{L1}(t_R)$$

$$= q_2\phi_s - \varrho_2\phi_R + 2\pi[q_2(\nu_{0s} + \nu_s)(t_R - \tau_\rho) - \varrho_2(\nu_{0L} + \nu_L)t_R]$$

$$+ q_2\eta_s(t_R - \tau_\rho) - \varrho_2\eta_L(t_R) \tag{8b}$$

The Doppler observation is essentially a measurement of phase at two different times. For example, from Equation 8a, the phase difference T seconds apart would be

$$\Phi_{F1}(t_R + T) - \Phi_{F1}(t_R)$$

A detailed expansion is written below as $\Delta\Phi$:

$$\Delta\Phi = \Phi_{F1}(t_R + T) - \Phi_{F1}(t_R)$$

$$\Delta\Phi = 2\pi\{q_1[\nu_{0s} + \nu_s(t_R + T)][t_R + T - \tau_\rho(t_R + T)] - q_1[\nu_{0s} + \nu_s(t_R)][t_R - \tau_\rho(t_R)]$$

$$- \varrho_1[\nu_{0L} + \nu_L(t_R + T)][t_R + T] + \varrho_2[\nu_{0L} + \nu_L(t_R)]\,t_R\}$$

$$+ q_1[\eta_s(t_R + T - \tau_\rho(t_R + T)) - \eta_s(t_R - \tau_\rho(t_R))] - \varrho_1[\eta_L(t_R + T) - \eta_L(t_R)] \tag{9}$$

This expression does not contain $q_1\phi_s$ or $\varrho_1\phi_R$ because these are constants and disappear in the subtraction. In like manner, if there were a channel bias term ϕ_{B1} in Equation 8a, it would also not appear in Equation 9. Therefore, this observation of $\Delta\Phi$ is not sensitive to a channel bias as long as the bias remains constant over the interval T.

It will be assumed that the frequency drifts contained in ν_s and ν_L are small enough so that the differences over a time T can be neglected. To demonstrate this, suppose $\dot{\nu}_s(t)$ is on the order of 4×10^{-11} Hz/s. This is a representative number obtained from the specification of the HP5065A Rubidium frequency standard[2]. The frequency drift for this unit is given as less than $\pm 1 \times 10^{-11}$ parts per month. Multiplying this by 10.23 MHz and dividing by the number of seconds per month produces the number stated above. Over the interval T, the difference $q_1[\dot{\nu}_s(t_R + T)(t_R + T) - \dot{\nu}_s(t_R)\,t_R]$ equals $4 \times 10^{-11} q_1 T$. Using $T = 60$ s and $q_1 = 154$, the resulting phase drift is $2\pi(4 \times 10^{-11})(154)(60) = 2.3 \times 10^{-6}$ radians, which is small enough to ignore. However, the random variations represented by $\eta(t)$ must be considered. Frequency instability is usually represented as a fractional frequency variation $\Delta f/f$ over an interval T. This implies a phase instability, which can be illustrated if the following operations are performed.

Let

$$\frac{\Delta f}{f}\,(T) = k$$

Then

$$\Delta f(T) = fk$$

and

$$\eta(t_R + T) - \eta(t_R) = \int_{t_R}^{t_R + T} \Delta f dt = fk \int_{t_R}^{t_R + T} dt = fT \frac{\Delta f}{f}(T)$$

Therefore, the drift due to the random contributions from the local reference frequency standard [assuming $T = 60$ s, $\Delta f/f(T) = 1 \times 10^{-12}$, $f = 5 \times 10^6$ Hz and $\varrho_1 = 315$] is $2\pi(10^{-12})(315)(5 \times 10^6)(60) = 0.47$ rad. This magnitude of phase instability is considerable and constitutes a major source of error in determining the phase difference $\Delta\Phi$. This phase noise will be collected and represented by the parameter ψ where

$$\psi = q_1[\eta_r(t_R + T - \tau_{p_r}(t_R + T)) - \eta_r(t_R - \tau_{p_r}(t_R))] - \varrho_1[\eta_t(t_R + T) - \eta_t(t_R)] \tag{10}$$

Since $\nu_r(t)$ and $\nu_t(t)$ were shown to vary little in an interval T, equation 9 can be simplified to

$$\Delta\Phi(t_R + T) = 2\pi\{q_1(\nu_{0r} + \nu_r)[T + \tau_{p_r}(t_R) - \tau_{p_t}(t_R + T)] - \varrho_1(\nu_{0t} + \nu_t)T\} + \psi$$

Division of $\Delta\Phi$ by 2π produces a number N_1 which is the Doppler count (the number of cycles in the interval T).

$$N_1 = \frac{\Delta\Phi(t_R + T)}{2\pi} = q_1(\nu_{0r} + \nu_r)[T + \tau_{p_r}(t_R) - \tau_{p_t}(t_R + T)] - \varrho_1(\nu_{0t} + \nu_t)T + \frac{\psi}{2\pi} \tag{11}$$

This is easily rearranged to place the difference in τ_p's on the left hand side.

$$\tau_{p_r}(t_R) - \tau_{p_t}(t_R + T) = \frac{1}{q_1(\nu_{0r} + \nu_r)}\left[N_1 - (q_1(\nu_{0r} + \nu_r)T - \varrho_1(\nu_{0t} + \nu_t)T) - \frac{\psi}{2\pi}\right] \tag{12}$$

In Equation 12, N_1 is the observation. The rest of the terms in the brackets represent that portion of the count that is due to the Doppler offset and the instability of the frequency reference.

Let us hypothesize that the propagation delay $\tau_p(t)$ is composed of the geometric slant range $r(t)$ and the ionospheric delay $I(t)$, which were introduced earlier. If this is substituted into Equation 12, the result is

$$r(t_R) - r(t_R + T) + I_r(t_R) - I_t(t_R + T) = c\left\{\frac{N_1 - [q_1(\nu_{0r} + \nu_r)T - \varrho_1(\nu_{0t} + \nu_t)T] - \psi_1/2\pi}{q_1(\nu_{0r} + \nu_r)}\right\} \tag{13a}$$

In like manner, an expression for I_2 can be developed:

$$r(t_R) - r(t_R + T) + I_r(t_R) - I_t(t_R + T) = c\left\{\frac{N_2 - [q_2(\nu_{0r} + \nu_r)T - \varrho_2(\nu_{0t} + \nu_t)T] - \psi_2/2\pi}{q_2(\nu_{0r} + \nu_r)}\right\} \tag{13b}$$

Since the geometric range $r(t)$ will be common to the two frequencies, it can be eliminated by subtracting Equation 13a from Equation 13b.

$$I_r(t_R) - I_t(t_R + T) - [I_r(t_R) - I_t(t_R + T)]$$

$$= \frac{c}{\nu_{0r} + \nu_r}\left\{\frac{N_1}{q_1} - \frac{N_2}{q_2} + (\nu_{0t} + \nu_t)T\begin{bmatrix}\varrho_1 & \varrho_2\\ q_1 & q_2\end{bmatrix}\frac{1}{2\pi}\begin{pmatrix}\psi_1 & \psi_2\\ q_1 & q_2\end{pmatrix}\right\} \tag{14}$$

This expression equates the part of the range that is frequency dependent, on the left, to the observations N_1, N_2, and T on the right. The ionosphere can be modeled by expressing the quantity $I(t)$ by an integral expression[3].

$$I(t_R) = \frac{-1}{2\omega_1^2} \int_{r_s(t_R)}^{r_s(t_R)} \frac{\omega^2(r)\, r dr}{(r^2 - k^2)^{1/2}} \tag{15}$$

where

$r_s(t_R)$ = satellite position at t_R
$r_R(t_R)$ = receiver position at $t_R + \tau$,
$\omega_1 = 2\pi q_1(\nu_{0L} + \nu_L)$

A similar expression can be written for $I_1(t_R + T)$ having the limits $r_s(t_R + T)$ and $r_R(t_R + T)$. The transmitted frequency appears only in the constant coefficient ω_1. The difference $I_1(t_R) - I_1(t_R + T)$ can be written as the difference of two integrals like Equation (15).

$$I_1(t_R) - I_1(t_R + T) = \frac{-1}{2\omega_1^2} \left\{ \int_{r_s(t_R)}^{r_s(t_R)} \frac{\omega^2(r)\, r dr}{(r^2 - k^2)^{1/2}} - \int_{r_R(t_R+T)}^{r_s(t_R+T)} \frac{\omega_R^2(r)\, r dr}{(r^2 - k^2)^{1/2}} \right\} \tag{16}$$

The expression in braces will be identical for I_2, and so it can be redefined as a constant I such that

$$I \quad \int_{r_s(t_R)}^{r_s(t_R)} \frac{\omega^2(r)\, r dr}{(r^2 - k^2)^{1/2}} - \int_{r_R(t_R+T)}^{r_s(t_R+T)} \frac{\omega^2(r)\, r dr}{(r^2 - k^2)^{1/2}} \tag{17}$$

Then Equation 16 can be simplified to the following form:

$$I_1(t_R) - I_1(t_R + T) = \frac{1}{2\omega_1^2} I$$

Likewise,

$$I_2(t_R) - I_2(t_R + T) = \frac{1}{2\omega_2^2} I$$

Inserting these into Equation 14 and solving for I produces an empirical result for the value of the two integrals defined in Equation 17.

$$I = \frac{8\pi^2 c q_1^2 q_2^2}{q_1^2 - q_2^2} (\nu_{0L} - \nu_L) \left\{ \frac{N_1}{q_1} - \frac{N_2}{q_2} + (\nu_{0L} + \nu_L) T \left[\frac{\varrho_1}{q_1} - \frac{\varrho_2}{q_2} \right] - \frac{1}{2\pi} \left[\frac{\psi_1}{q_1} - \frac{\psi_2}{q_2} \right] \right\} \tag{18}$$

This can now be substituted into either Equation 13a or Equation 13b to produce an ionosphere-corrected observation of the range difference $r(t_R) - r(t_R + T)$. These are written as Equations 19a and 19b:

$$r(t_R) - r(t_R + T) = c \left\{ \frac{N_1 - [q_1(\nu_{0L} + \nu_L) T - \varrho_1(\nu_{0L} + \nu_L) T] - \psi_1 2\pi}{q_1(\nu_{0L} + \nu_L)} \right\} + \frac{I}{8\pi^2 q_1^2 (\nu_{0L} + \nu_L)^2} \tag{19a}$$

$$r(t_R) - r(t_R + T) = c\left\{\frac{N_2 - [q_2(\nu_{0s} + \nu_s)T - \varrho_2(\nu_{0L} + \nu_L)T] - \psi_2/2\pi}{q_2(\nu_{0s} + \nu_s)}\right\} + \frac{I}{8\pi^2 q_2^2(\nu_{0s} + \nu_s)^2} \tag{19a}$$

ERROR ANALYSIS

Now that the conversion from raw Doppler counts to range difference has been developed, it will be informative to investigate the sensitivity of these expressions to errors in the measurements. The last term in Equation 19 can be combined with Equation 18 to eliminate some of the constants. This new parameter is defined in Equations 20a and 20b:

$$J_a = \frac{I}{8\pi^2 q_1^2(\nu_{0s} + \nu_s)^2} = \frac{cq_2^2}{(q_1^2 - q_2^2)(\nu_{0s} + \nu_s)}\left\{\frac{N_1}{q_1} - \frac{N_2}{q_2} + (\nu_{0L} + \nu_L)\right.$$
$$\left. T\left[\frac{\varrho_1}{q_1} - \frac{\varrho_2}{q_2}\right] - \frac{1}{2\pi}\left[\frac{\psi_1}{q_1} - \frac{\psi_2}{q_2}\right]\right\} \tag{20a}$$

$$J_b = \frac{I}{8\pi^2 q_2^2(\nu_{0s} + \nu_s)^2} = \frac{cq_1^2}{(q_1^2 - q_2^2)(\nu_{0s} + \nu_s)}\left\{\frac{N_1}{q_1} - \frac{N_2}{q_2} + (\nu_{0L} + \nu_L)\right.$$
$$\left. T\left[\frac{\varrho_1}{q_1} - \frac{\varrho_2}{q_2}\right] - \frac{1}{2\pi}\left[\frac{\psi_1}{q_1} - \frac{\psi_2}{q_2}\right]\right\} \tag{20b}$$

The parameters that will be considered to be uncertain are ν_s, ν_L, N_1, N_2, ψ_1, ψ_2 and T.

Special consideration must be given to ψ_1 and ψ_2, since they are highly correlated. The form of Equation 10 can be used to describe both ψ_1 and ψ_2.

$$\psi_1 = q_1[\eta_s(t_R + T - \tau_\mu) - \eta_s(t_R - \tau_\mu)] - \varrho_1[\eta_L(t_R + T) - \eta_L(t_R)]$$

$$\psi_2 = q_2[\eta_s(t_R + T - \tau_\mu) - \eta_s(t_R - \tau_\mu)] - \varrho_2[\eta_L(t_R + T) - \eta_L(t_R)]$$

Using these, the quantity $\psi_1/q_1 - \psi_2/q_2$, which is common to both J_a and J_b, can be written:

$$\frac{\psi_1}{q_1} - \frac{\psi_2}{q_2} = [\eta_s(t_R + T - \tau_\mu) - \eta_s(t_R - \tau_\mu)] - \frac{\varrho_1}{q_1}[\eta_L(t_R + T) - \eta_L(t_R)]$$
$$- \{[\eta_s(t_R + T - \tau_\mu) - \eta_s(t_R - \tau_\mu)] - \frac{\varrho_2}{q_2}[\eta_L(t_R + T) - \eta_L(t_R)]\}$$

Here the satellite phase noise contribution combines to add to zero, which leaves only a reduced contribution from the local frequency reference.

$$\frac{\psi_1}{q_1} - \frac{\psi_2}{q_2} = \left(\frac{\varrho_2}{q_2} - \frac{\varrho_1}{q_1}\right)(\eta_L(t_R + T) - \eta_L(t_R))$$

$$= -1.06 \times 10^{-5}[\eta_L(t_R + T) - \eta_L(t_R)]$$

Thus, in addition to partials of J_a and J_b with respect to ψ_1 and ψ_2, the partials $\partial\psi_1/\partial\eta$ and $\partial\psi_2/\partial\eta$ will be defined.

$$\frac{\partial\psi_1}{\partial\eta} = q_1\left(\frac{\varrho_2}{q_2} - \frac{\varrho_1}{q_1}\right)$$

$$\frac{\partial\psi_2}{\partial\eta} = -\frac{\partial\psi_1}{\partial\eta}\quad\frac{q_2}{q_1}$$

where

$$\eta = [\eta_L(t_R + T) - \eta_L(t_R)]$$

The partials of J with respect to the seven parameters are written below:

$$\frac{\partial J_a}{\partial\nu_s} = \frac{-cq_2^2}{q_1^2 - q_2^2}\quad\frac{1}{(\nu_{0s} + \nu_s)^2}\quad\left\{\frac{N_1}{q_1} - \frac{N_2}{q_2} + (\nu_{0t} + \nu_t)\right.$$

$$\left. T\left[\frac{\varrho_1}{q_1} - \frac{\varrho_2}{q_2}\right] - \frac{1}{2\pi}\left[\frac{\psi_1}{q_1} - \frac{\psi_2}{q_2}\right]\right.$$

$$\frac{\partial J_b}{\partial\nu_s} = \frac{-cq_1^2}{q_1^2 - q_2^2}\quad\frac{1}{(\nu_{0s} + \nu_s)^2}\quad\left\{\frac{N_1}{q_1} - \frac{N_2}{q_2} + (\nu_{0t} + \nu_t)\right.$$

$$\left. T\left[\frac{\varrho_1}{q_1} - \frac{\varrho_2}{q_2}\right] - \frac{1}{2\pi}\left[\frac{\psi_1}{q_1} - \frac{\psi_2}{q_2}\right]\right\}$$

$$\frac{\partial J_a}{\partial\nu_L} = \frac{cq_2^2}{(q_1^2 - q_2^2)(\nu_{0s} + \nu_s)}\,T\left[\frac{\varrho_1}{q_1} - \frac{\varrho_2}{q_2}\right]$$

$$\frac{\partial J_a}{\partial\nu_t} = \frac{cq_1^2}{(q_1^2 - q_2^2)(\nu_{0s} + \nu_s)}\,T\left[\frac{\varrho_1}{q_1} - \frac{\varrho_2}{q_2}\right]$$

$$\frac{\partial J_a}{\partial N_1} = \frac{cq_2^2}{(q_1^2 - q_2^2)(\nu_{0s} + \nu_s)q_1}$$

$$\frac{\partial J_b}{\partial N_1} = \frac{cq_1}{(q_1^2 - q_2^2)(\nu_{0s} + \nu_s)}$$

$$\frac{\partial J_a}{\partial N_2} = \frac{-cq_2}{(q_1^2 - q_2^2)(\nu_{0s} + \nu_s)}$$

$$\frac{\partial J_b}{\partial N_2} = \frac{-cq_1^2}{(q_1^2 - q_2^2)(\nu_{0s} + \nu_s)q_2}$$

$$\frac{\partial J_a}{\partial \psi_1} = \frac{-cq_2^2}{(q_1^2 - q_2^2)(\nu_{0s} + \nu_s)2\pi q_1}$$

$$\frac{\partial J_b}{\partial \psi_1} = \frac{-cq_1}{(q_1^2 - q_2^2)(\nu_{0s} + \nu_s)2\pi}$$

$$\frac{\partial J_a}{\partial \psi_2} = \frac{cq_2}{(q_1^2 - q_2^2)(\nu_{0s} + \nu_s)2\pi}$$

$$\frac{\partial J_b}{\partial \psi_2} = \frac{cq_1^2}{(q_1^2 - q_2^2)(\nu_{0s} + \nu_s)2\pi q_2}$$

$$\frac{\partial J_a}{\partial T} = \frac{cq_2^2(\nu_{0L} + \nu_L)}{(q_1^2 - q_2^2)(\nu_{0s} + \nu_s)} \left[\frac{\varrho_1}{q_1} - \frac{\varrho_2}{q_2}\right]$$

$$\frac{\partial J_b}{\partial T} = \frac{cq_1^2(\nu_{0L} + \nu_L)}{(q_1^2 - q_2^2)(\nu_{0s} + \nu_s)} \left[\frac{\varrho_1}{q_1} - \frac{\varrho_2}{q_2}\right]$$

The error in J due to these parameters is obtained from the total derivative:

$$dJ = \frac{\partial J}{\partial \nu_s} d\nu_s + \frac{\partial J}{\partial \nu_L} d\nu_L + \frac{\partial J}{\partial N} dN + \frac{\partial J}{\partial \psi} d\psi + \frac{\partial J}{\partial T} dT \tag{21}$$

If values are assigned to the constants, the sensitivity of J to each of the parameters can be evaluated. The appropriate constants are

$\nu_{0s} = 10.23 \times 10^6$ Hz
$\nu_s = 0$
$\nu_{0l} = 5.00 \times 10^6$ Hz
$\nu_l = 0$
$c = 2.99792458 \times 10^8$ m/s
$q_1 = 154$, $q_2 = 120$
$\varrho_1 = 315.07825$, $\varrho_2 = 245.51425$
$T = 60$ s
$N_1 = N_2 = 1725000$
$\psi_1 = \psi_2 = 0$

Using these, the numerical values for the partials are

$$\frac{\partial J_a}{\partial \nu_s} = -0.0992 \text{ m/Hz}, \quad \frac{\partial J_b}{\partial \nu_s} = -0.1634 \text{ m/Hz}$$

$$\frac{\partial J_a}{\partial \nu_l} = 0.0288 \text{ m/Hz}, \quad \frac{\partial J_b}{\partial \nu_l} = 0.0474 \text{ m/Hz}$$

$$\frac{\partial J_a}{\partial N_1} = 0.2941 \text{ m/count}, \quad \frac{\partial J_b}{\partial N_1} = 0.4844 \text{ m/count}$$

$$\frac{\partial J_a}{\partial N_2} = -0.3775 \text{ m/count}, \quad \frac{\partial J_b}{\partial N_2} = -0.6217 \text{ m/count}$$

$$\frac{\partial J_a}{\partial \psi_1} = -0.0468 \text{ m/rad}, \quad \frac{\partial J_b}{\partial \psi_1} = -0.0771 \text{ m/rad}$$

$$\frac{\partial J_a}{\partial \psi_2} = 0.0601 \text{ m/rad}, \quad \frac{\partial J_b}{\partial \psi_2} = 0.0989 \text{ m/rad}$$

$$\frac{\partial J_a}{\partial T} = 2396.0128 \text{ m/s}, \quad \frac{\partial J_b}{\partial T} = 3946.1000 \text{ m/s}$$

In a similar fashion, Equation 19 allows the definition of D_a and D_b as the uncorrected L_1 and L_2 range difference observations:

$$D_a = c\left\{\frac{N_1 - [q_1(\nu_{0s} + \nu_s)T - \varrho_1(\nu_{0L} + \nu_L)T] - \psi_1/2\pi}{q_1(\nu_{0s} + \nu_s)}\right\} \tag{22a}$$

$$D_b = c\left\{\frac{N_2 - [q_2(\nu_{0s} + \nu_s)T - \varrho_2(\nu_{0L} + \nu_L)T] - \psi_2/2\pi}{q_2(\nu_{0s} + \nu_s)}\right\} \tag{22b}$$

The partials of D_a and D_b with respect to the same set of parameters are

$$\frac{\partial D_a}{\partial \nu_s} = \frac{-cT}{\nu_{0s} + \nu_s} - \frac{c}{q_1(\nu_{0s} + \nu_s)^2}\left\{N_1 - [q_1(\nu_{0s} + \nu_s)T - \varrho_1(\nu_{0L} + \nu_L)T] - \frac{\psi_1}{2\pi}\right\}$$

$$\frac{\partial D_b}{\partial \nu_s} = \frac{-cT}{\nu_{0s} + \nu_s} - \frac{c}{q_2(\nu_{0s} + \nu_s)^2}\left\{N_2 - [q_2(\nu_{0s} + \nu_s)T - \varrho_2(\nu_{0L} + \nu_L)T] - \frac{\psi_2}{2\pi}\right\}$$

$$\frac{\partial D_a}{\partial \nu_L} = \frac{-c\varrho_1 T}{q_1(\nu_{0s} + \nu_s)}$$

$$\frac{\partial D_b}{\partial \nu_L} = \frac{-c\varrho_2 T}{q_2(\nu_{0s} + \nu_s)}$$

$$\frac{\partial D_b}{\partial N_1} = \frac{\partial D_a}{\partial N_2} = 0$$

$$\frac{\partial D_a}{\partial N_1} = \frac{c}{q_1(\nu_{0s} + \nu_s)}, \quad \frac{\partial D_b}{\partial N_2} = \frac{c}{q_2(\nu_{0s} + \nu_s)}$$

$$\frac{\partial D_a}{\partial \psi_1} = \frac{-c}{2\pi q_1(\nu_{0s} + \nu_s)}$$

$$\frac{\partial D_b}{\partial \psi_2} = \frac{-c}{2\pi q_2(\nu_{0s} + \nu_s)}$$

$$\frac{\partial D_b}{\partial \psi_1} = \frac{\partial D_a}{\partial \psi_2} = 0$$

$$\frac{\partial D_a}{\partial T} = \frac{c}{q_1(\nu_{0s} + \nu_s)} [- q_1(\nu_{0s} + \nu_s) + \varrho_1(\nu_{0L} + \nu_L)]$$

$$\frac{\partial D_b}{\partial T} = \frac{c}{q_2(\nu_{0s} + \nu_s)} [- q_2(\nu_{0s} + \nu_s) + \varrho_2(\nu_{0L} + \nu_L)]$$

The sensitivity of D to each of the parameters can be evaluated using the same set of constants as before. The partials with respect to ν_s are a function of the actual Doppler count and are a minimum when the Doppler frequency is zero. This is because the terms

$$q_1(\nu_{0s} + \nu_s)\ T - \varrho_1(\nu_{0L} + \nu_L)T$$

and

$$q_2(\nu_{0s} + \nu_s)\ T - \varrho_2(\nu_{0L} + \nu_L)T$$

equal 1,725,000. When $N_1 = N_2 = 1{,}725{,}000$, the term in braces is zero. In order to represent the worst case, N will be adjusted to the equivalent of a ± 4000 Hz Doppler frequency in these two partials only.

$$\frac{\partial D_a}{\partial \nu_s} = -1758.3036 \text{ m/Hz}, \qquad \frac{\partial D_b}{\partial \nu_s} = -1758.3048 \text{ m/Hz}$$

$$\frac{\partial D_a}{\partial \nu_L} = -3597.4143 \text{ m/Hz}, \qquad \frac{\partial D_b}{\partial \nu_L} = -3597.3957 \text{ m/Hz}$$

$$\frac{\partial D_a}{\partial N_1} = 0.1903 \text{ m/count}, \qquad \frac{\partial D_b}{\partial N_2} = 0.2442 \text{ m/count}$$

$$\frac{\partial D_a}{\partial \psi_1} = 0.0303 \text{ m/rad}, \qquad \frac{\partial D_b}{\partial \psi_2} = 0.0389 \text{ m/rad}$$

$$\frac{\partial D_a}{\partial T} = -5470.9 \text{ m/s}, \qquad \frac{\partial D_b}{\partial T} = -7021.0 \text{ m/s}$$

A comparison of the values of the partials for D and J indicate that, in all cases, the greatest contribution to the observation of a range difference will come from the D's not the J's.

Equations 19a and 19b are equivalent; therefore, the range difference observation can be obtained from either. However, inspection of Equations 20a and 20b shows that, for a given error in any of the quantities in the braces, the resulting error in J_a will be less than in J_b. This is because of

the different multiplying factors involved. Also, Equations 22a and 22b indicate that an error in the count N, time interval T, or in the phase noise ψ, will be less in D_a than in D_b. Again, this is because of the multiplying factors. This conclusion is also apparent in the values of the partials listed above. In all cases, the partials of D_a and J_a are less, respectively than those of D_b and J_b. However, the error propagated into the ionospheric corrected range difference observation due to errors in N or ψ is the same irrespective of whether D_a or D_b is used as the basis of the measurement.

This can be illustrated in the case of an error in N by employing the appropriate partials. The partials derived from Equations 19a and 20a are

$$\Delta r = \frac{\partial D_a}{\partial N_1}\Delta N_1 + \frac{\partial J_a}{\partial N_1}\Delta N_1 + \frac{\partial J_a}{\partial N_2}\Delta N_2$$

$$\Delta r = \frac{c}{q_1(\nu_{0s}+\nu_s)}\Delta N_1 + \frac{cq_2^2}{(q_1^2-q_2^2)(\nu_{0s}+\nu_s)q_1}\Delta N_1 + \frac{(-cq_2)}{(q_1^2-q_2^2)(\nu_{0s}+\nu_s)}\Delta N_2$$

Assuming that $\Delta N_1 = \Delta N_2$, this results in

$$\Delta r = c\left[\frac{q_1-q_2}{(q_1^2-q_2^2)(\nu_{0s}+\nu_s)}\right]\Delta N$$

A similar expression can be written from Equations 19b and 20b:

$$\Delta r = \frac{\partial D_b}{\partial N_2}\Delta N_2 + \frac{\partial J_b}{\partial N_1}\Delta N_1 + \frac{\partial J_b}{\partial N_2}\Delta N_2$$

$$\Delta r = \frac{c}{q_2(\nu_{0s}+\nu_s)}\Delta N_2 + \frac{cq_1}{(q_1^2-q_2^2)(\nu_{0s}+\nu_s)}\Delta N_1 - \frac{cq_1^2}{(q_1^2-q_2^2)(\nu_{0s}+\nu_s)}\Delta N_2$$

Assuming that $\Delta N_1 = \Delta N_2$, this also results in

$$\Delta r = c\left[\frac{q_1-q_2}{(q_1^2-q_2^2)(\nu_{0s}+\nu_s)}\right]\Delta N$$

A similar result is obtained when the error parameter is ψ. Consequently, if the primary error source is due to uncertainties in N or ψ, either expression produces an equivalent error in the final range difference calculation. Since this is the case, the next section will dwell on evaluating the errors from D_a and J_a.

EXPECTED OBSERVATIONAL ERROR

An estimate of the error in each observation can be made by using the preceding partial derivatives and the expected errors in each of the parameters considered. These expected errors will be based upon the considerations discussed in the following paragraphs.

The frequency offset ν_s will be expected to drift at a rate of about 4×10^{-18} parts/s. Using the nominal frequency for ν_{0s}, this is about 4.1×10^{-11} Hz/s, or 2.5×10^{-9} Hz in a 60-s observation period. The frequency offset ν_l will be expected to vary less than 1.2×10^{-18} parts of ν_{0L}, or 3.5×10^{-10} Hz. This latter number is from the HP5061A-004 specification.

The Doppler count accuracy is limited by the resolution of the fractional time interval counter. At the nominal offset frequency of 28750 Hz, the $\pm$10-ns resolution of the time interval counter is equivalent to approximately $2 \times 10^{-8} \times 28750$ of a count. This is 5.75×10^{-4} cycle, or 3.6×10^{-3} rad. The white noise from the receiver is on the order of 0.1 rad rms, so the limiting factor is not the counter, but this receiver noise. Thus, the Doppler count error will be taken as 0.1 rad, or 0.016 count, in the rest of this development. This error source should decrease with increasing signal strength.

The phase noise ψ comes primarily from the frequency standards. Equation 10 shows that it is a composite of contributions from the satellite and local references. The satellite will be assigned an Allen variance over a minute of 2×10^{-12} (Reference 4), while the local reference will be assigned 1×10^{-12}. The phase variation over 1 min can be estimated from Equation 10 in the same manner as before. This expression when evaluated becomes

$$q_1[\eta_s(t_R + T) - \eta_s(t_R)] = 2\pi(2 \times 10^{-12})\ (154)\ (10.23 \times 10^6)\ (60) = 1.19 \text{ rad}$$

In a similar fashion, the result for the local clock is

$$\varrho_1[\eta_l(t_R + T) - \eta_l(t_R)] = 2\pi(1 \times 10^{-12})\ (3.15.08)\ (5 \times 10^6)\ (60) = 0.59 \text{ rad}$$

From both of these, the magnitude of $\Delta\psi = 1.33$ rad.

The accuracy of the Doppler count interval is correlated with the count itself, since the interval is triggered to begin and end by the zero crossings of the Doppler count. Since this signal has noise attached to it, there will be a corresponding uncertainty in the duration of the interval. Using the 0.1-rad figure as representative of the noise and the duration of the nominal Doppler cycle as 3.5×10^{-5} s, the time corresponding to 0.1 rad of this frequency is 5.5×10^{-7} s.

Finally the error in the observation will be calculated using the total derivative as in Equation 21.

$$\Delta J_a = \frac{\partial J_a}{\partial \nu_s}\Delta\nu_s + \frac{\partial J_a}{\partial \nu_l}\Delta\nu_l + \frac{\partial J_a}{\partial N_1}\Delta N_1 + \frac{\partial J_a}{\partial N_2}\Delta N_2 + \frac{\partial J_a}{\partial \psi_1}\Delta\psi_1 + \frac{\partial J_a}{\partial \psi_2}\Delta\psi_2 + \frac{\partial J_a}{\partial T}\Delta T$$

The magnitude of ΔJ_a is obtained from the square root of the sum of the squares of each of the terms above. A similar expression will be used for ΔD_a.

$$\Delta D_a = \frac{\partial D_a}{\partial \nu_s}\Delta\nu_s + \frac{\partial D_a}{\partial \nu_l}\Delta\nu_l + \frac{\partial D_a}{\partial N_1}\Delta N_1 + \frac{\partial D_a}{\partial \psi_1}\Delta\psi_1 + \frac{\partial D_a}{\partial T}\Delta T$$

The results of the calculation, term by term, follow:

$$\frac{\partial J_a}{\partial \nu_s}\Delta\nu_s = -2.5 \times 10^{-10} \text{ m}, \qquad \frac{\partial D_a}{\partial \nu_s}\Delta\nu_s = -4.4 \times 10^{-6} \text{ m}$$

$$\frac{\partial J_a}{\partial \nu_l}\Delta\nu_l = 1.0 \times 10^{-11} \text{ m}, \qquad \frac{\partial D_a}{\partial \nu_l}\Delta\nu_l = -1.3 \times 10^{-6} \text{ m}$$

$$\frac{\partial J_a}{\partial N_1}\ \Delta N_1 \quad 0.0047\ \text{m}, \qquad \frac{\partial D}{\partial N_1}\ \Delta N \quad 0.0030\ \text{m}$$

$$\frac{\partial J_a}{\partial N_2}\ \Delta N_2 = -0.0060\ \text{m}, \qquad \frac{\partial D}{\partial N_2}\ \Delta N_2 \quad 0$$

$$\frac{\partial J_a}{\partial \psi_1}\ \Delta\psi_1 = \frac{\partial J_a}{\partial \psi_1}\ \frac{\partial \psi_1}{\partial \eta}\ \Delta\eta = -8 \times 10^{-5}\ \text{m}, \qquad \frac{\partial D_a}{\partial \psi_1}\ \Delta\psi_1 = 0.040\ \text{m}$$

$$\frac{\partial J_a}{\partial \psi_2}\ \Delta\psi_2 = \frac{\partial J_a}{\partial \psi_2}\ \frac{\partial \psi_2}{\partial \eta}\ \Delta\eta = -8 \times 10^{-5}\ \text{m}, \qquad \frac{\partial D_a}{\partial \psi_2}\ \Delta\psi_2 = 0$$

$$\frac{\partial J_a}{\partial T}\ \Delta T = 0.0013\ \text{m}, \qquad \frac{\partial D_a}{\partial T}\ \Delta T = -0.0030\ \text{m}$$

It is interesting to see that the accuracy of the ionospheric correction is limited not by phase noise from the frequency standards, but by the errors in determining the Doppler counts N_1 and N_2. This noise comes primarily from random phase fluctuations in the receiver. If N_1 and N_2 are considered to be independent, then the magnitude of the noise expected on the ionospheric correction observation is

$$\Delta J_a \cong \left[\left(\frac{\partial J_a}{\partial N_1}\ \Delta N_1\right)^2 + \left(\frac{\partial J_a}{\partial N_2}\ \Delta N_2\right)^2\right]^{1/2}$$

$$\Delta J_a \cong 0.0076\ \text{m}$$

The contributions from the remaining parameters are small enough to ignore.

The error in the range difference observation, 4.02 cm, is dominated by the frequency standard phase noise. If this error source were reduced by a factor of 20 or more, then the limits would be set by the error in determination of the count and the exact interval of the count. This factor of 20 is equivalent to improving the Allen variance from 10^{-12} to 5×10^{-14} over the interval T and would be comparable to the performance expected from a Hydrogen Maser.

The levels of error in D_a and J_a predicted by the preceding analysis have been empirically verified by actual data. NAVSTARS 1 through 4 (SV's 4, 7, 6, and 8) were operational while the NGRS was at Yuma in 1979. The Doppler data that were obtained from all four satellites were processed so that 20-min segments were fitted to a third-degree polynomial using least squares. The residuals of this fit were used to determine an rms that is considered to be representative of the random fluctuations of the Doppler observations. Uncorrected L_1 Doppler data corresponding to D_a and the ionospheric correction to L_1, corresponding to J_a, were processed in the same way. The rms values of the residuals for D_a are plotted vs date in Figures 4 through 7, and the residuals for J_a are plotted in Figures 8 through 11.

Throughout these 44 days, the local frequency reference behaved normally, and so the jumps in the calculated rms (e.g., those in Figure 4 between days 45 and 54) are due to misbehavior of the SV4 frequency standard. Note, however, that during these nine days there is no evidence of anything amiss in Figure 8. This illustrates that the ionospheric correction is not sensitive to the phase noise of the frequency standards. This was the result predicted by the analysis of J_a. An especially graphic

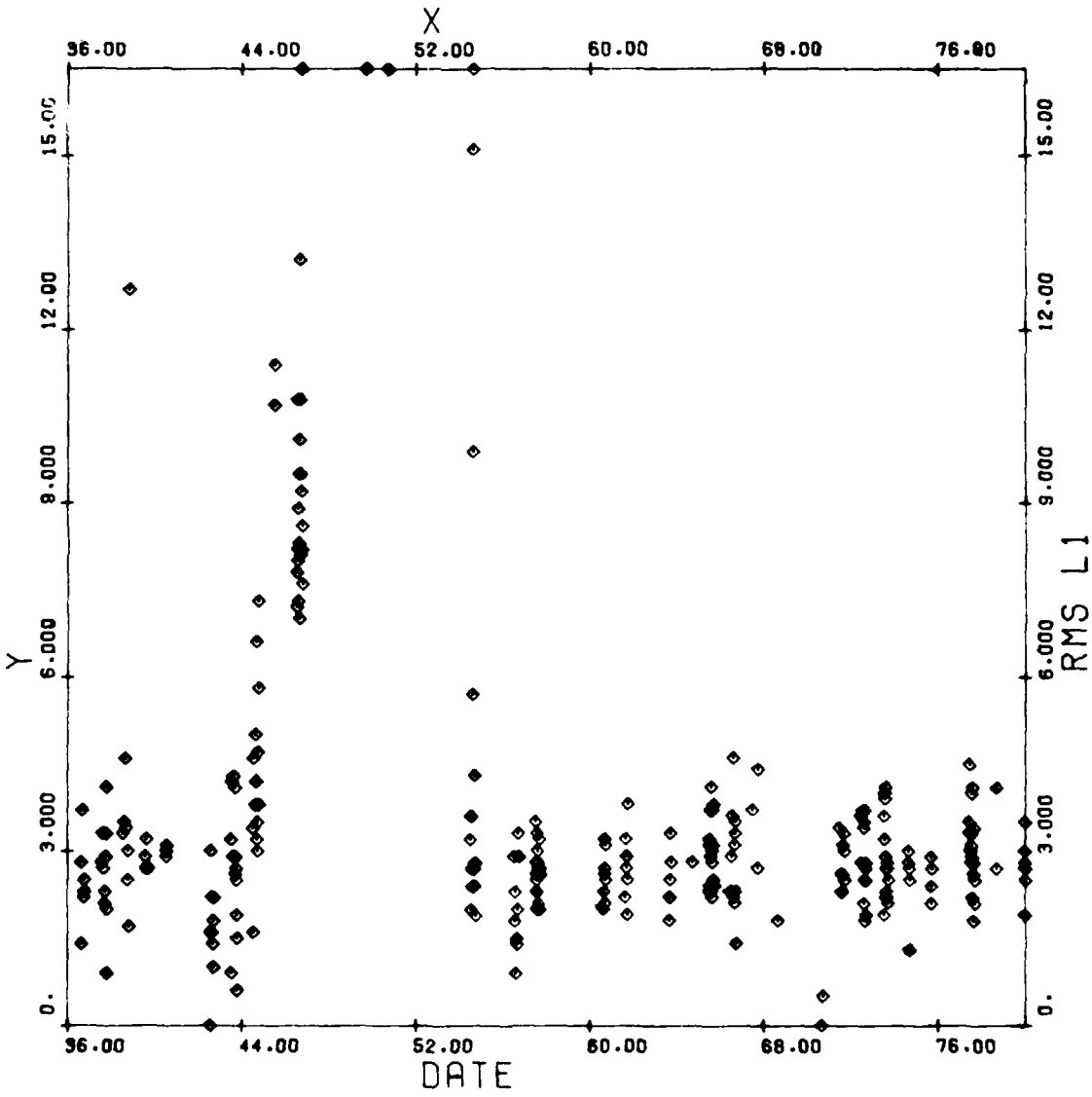

Figure 4. 20-Min L_1 Range Difference RMS (cm) Vs Date, GPS SV-4, Yuma Proving Grounds, Days 36-80 1979

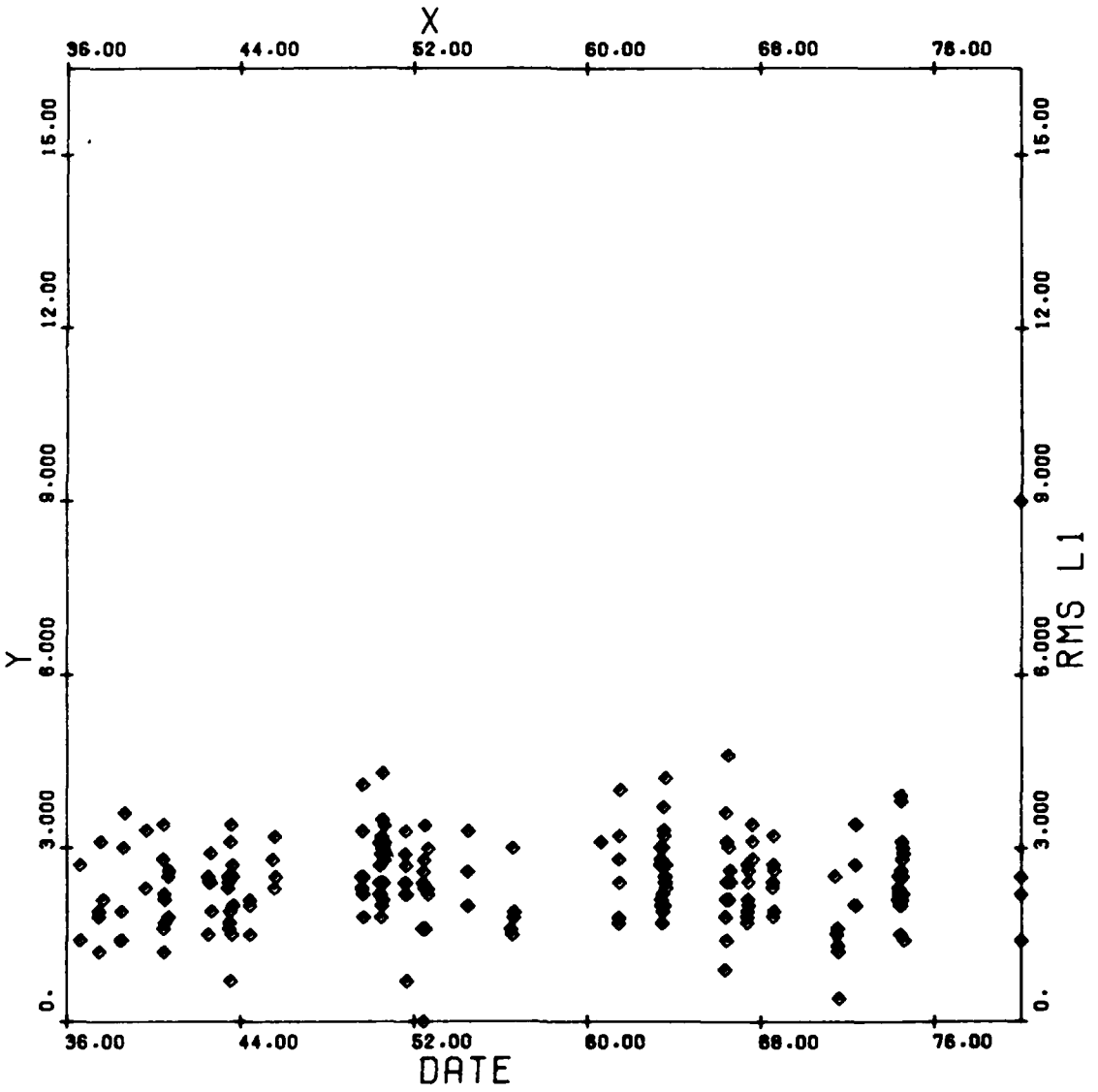

Figure 5. 20-Min L_1 Range Difference RMS (cm) Vs Date, GPS SV-6, Yuma Proving Grounds, Days 36-80 1979

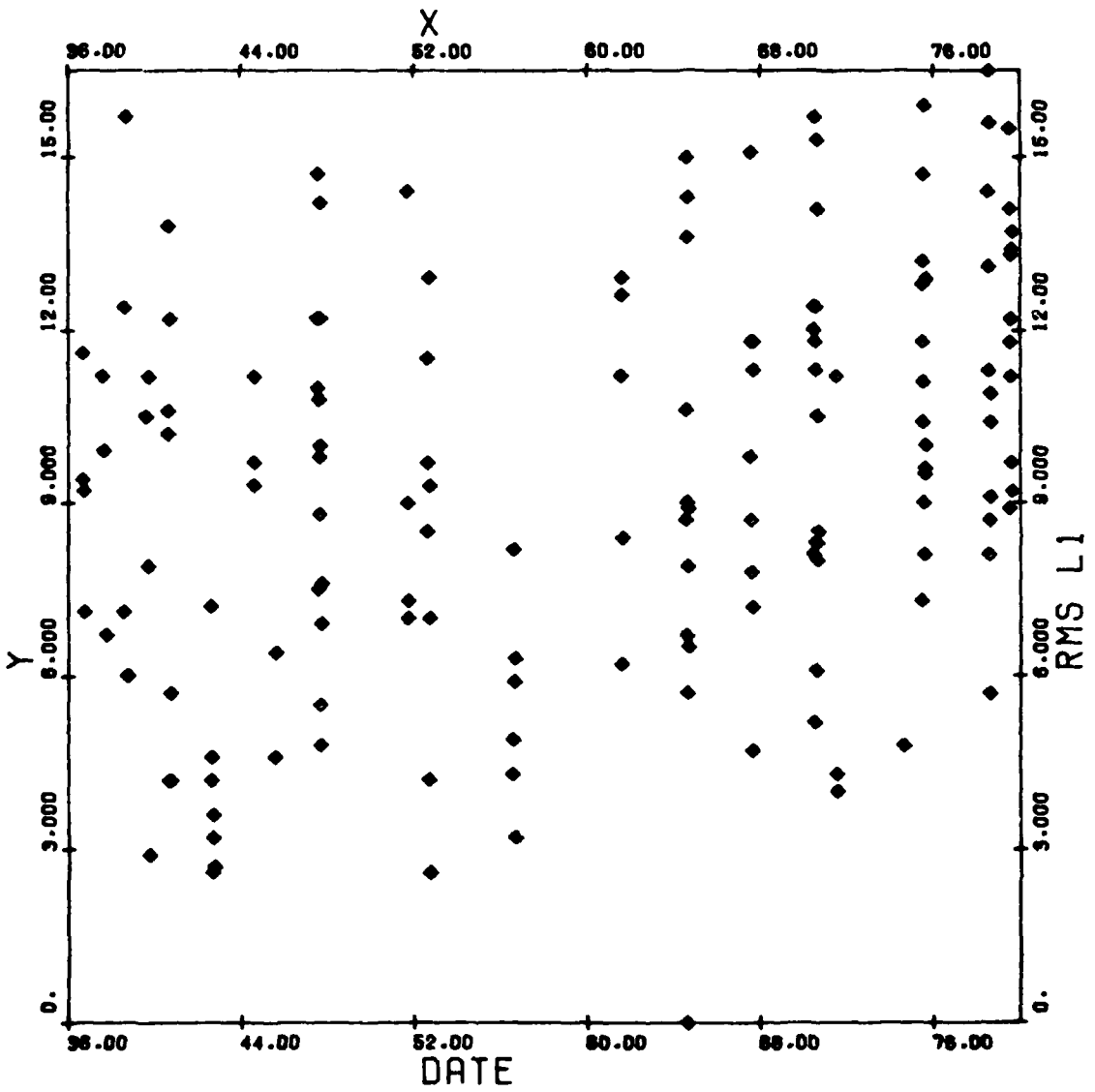

Figure 6. 20-Min L_1 Range Difference RMS (cm) Vs Date, GPS SV-7, Yuma Proving Grounds, Days 36-80 1979

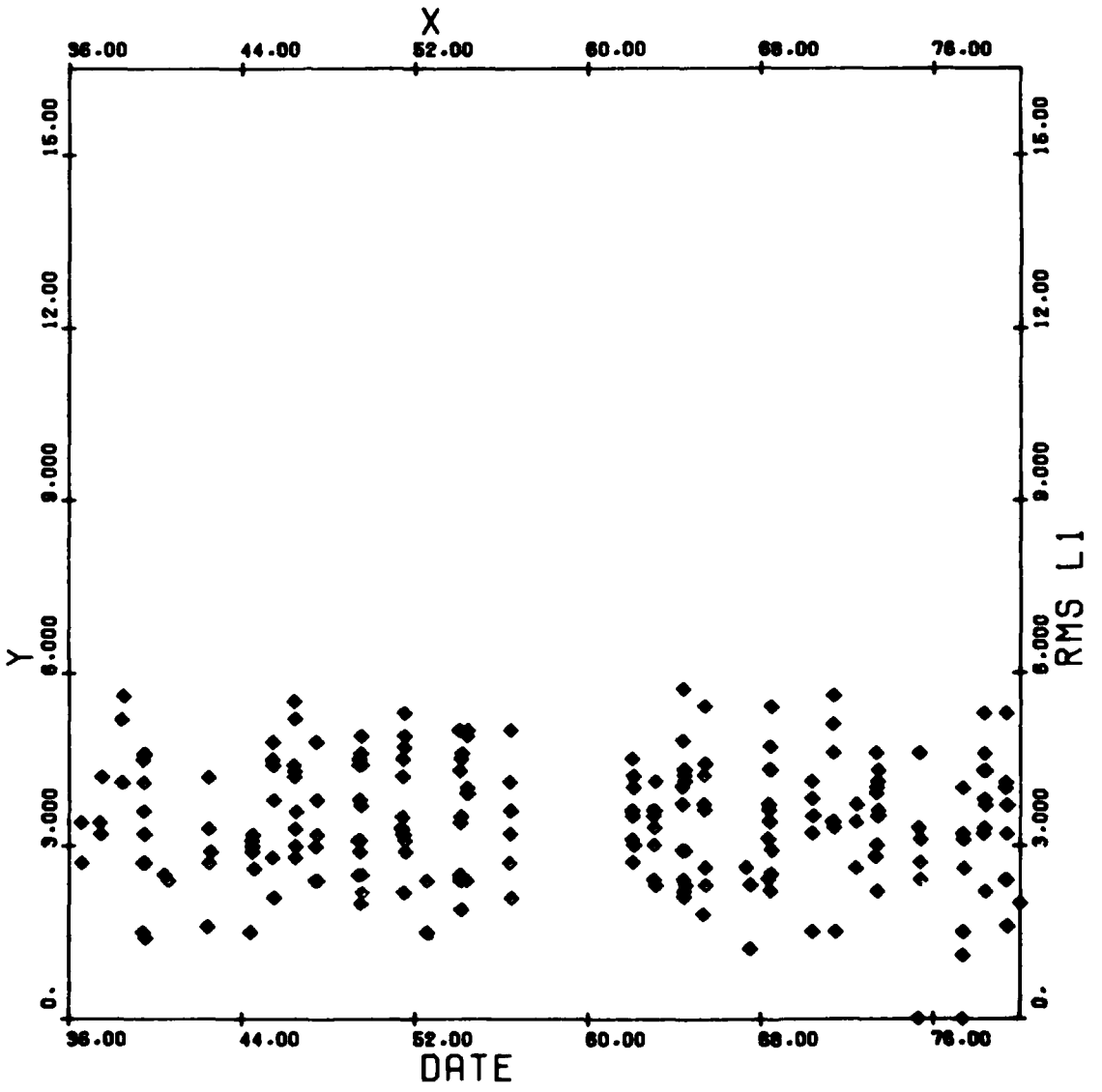

Figure 7. 20-Min L_1 Range Difference RMS (cm) Vs Date, GPS SV-8, Yuma Proving Grounds, Days 36-80 1979

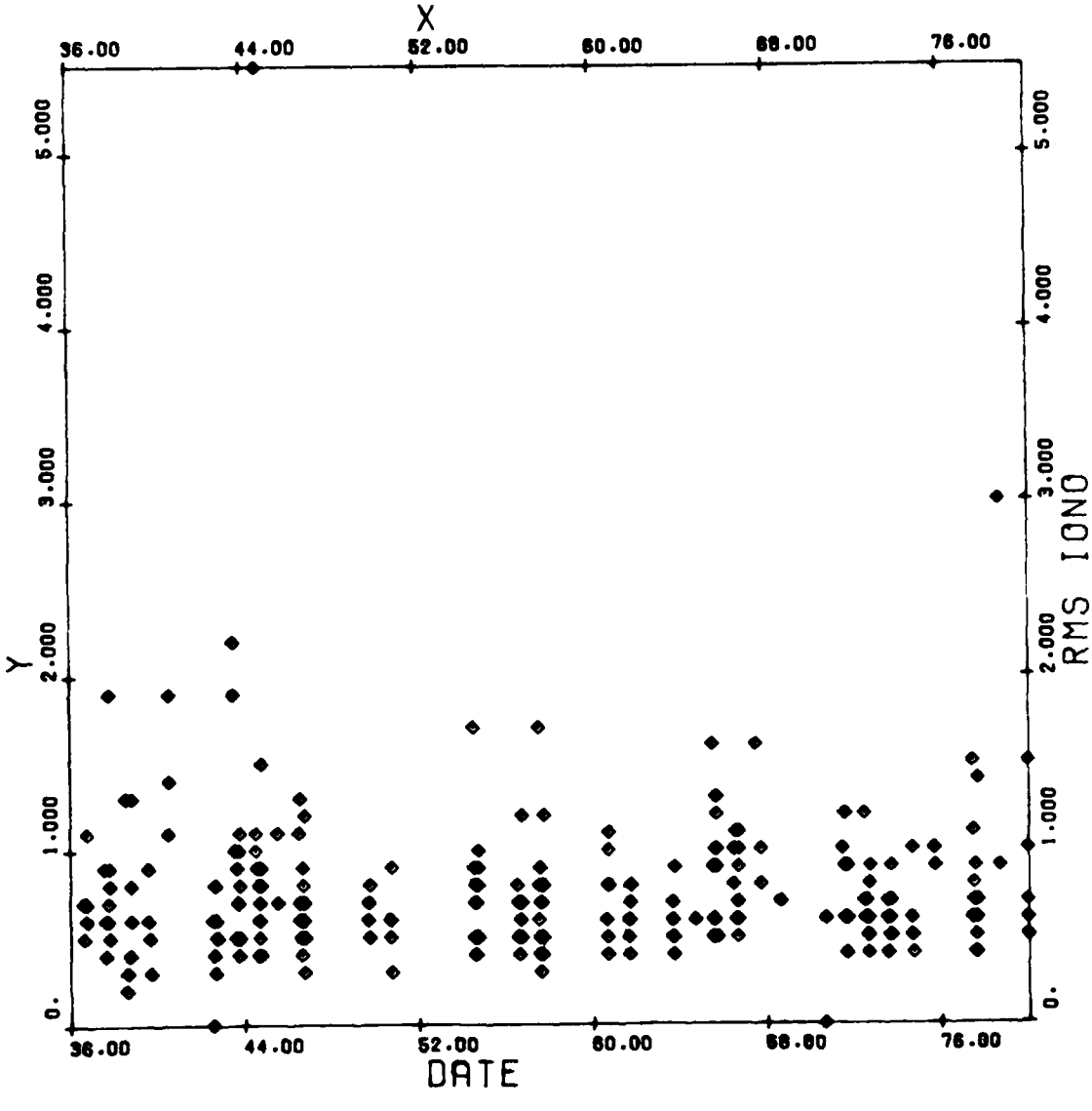

Figure 8. 20-Min Ionospheric Correction to L_1 RMS (cm) Vs Date, GPS SV-4, Yuma Proving Grounds, Days 36-80 1979

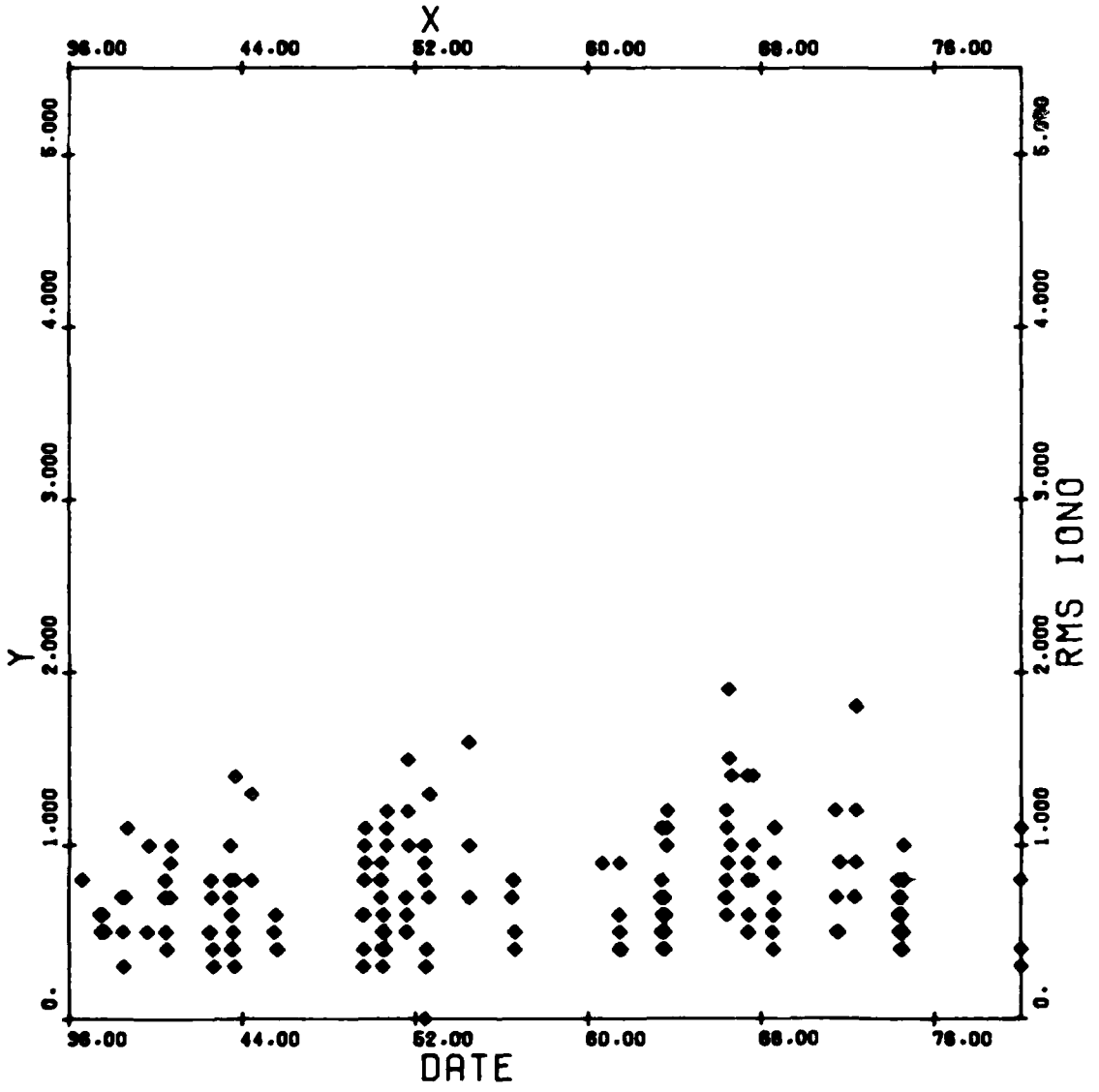

Figure 9. 20-Min Ionospheric Correction to L_1 RMS (cm) Vs Date, GPS SV-6, Yuma Proving Grounds, Days 36-80 1979

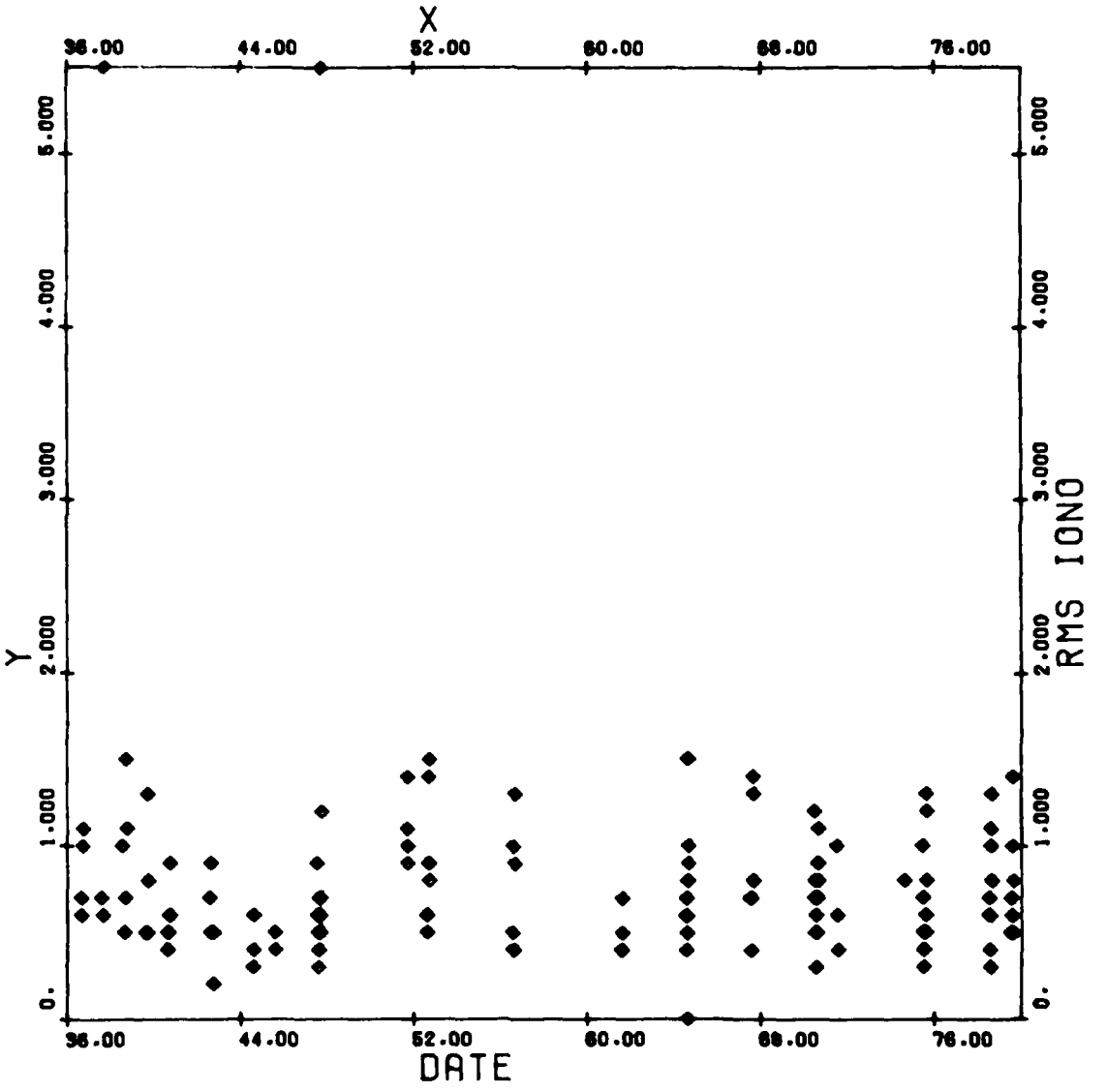

Figure 10. 20-Min Ionospheric Correction to L_1 RMS (cm) Vs Date, GPS SV-7, Yuma Proving Grounds, Days 36-80 1979

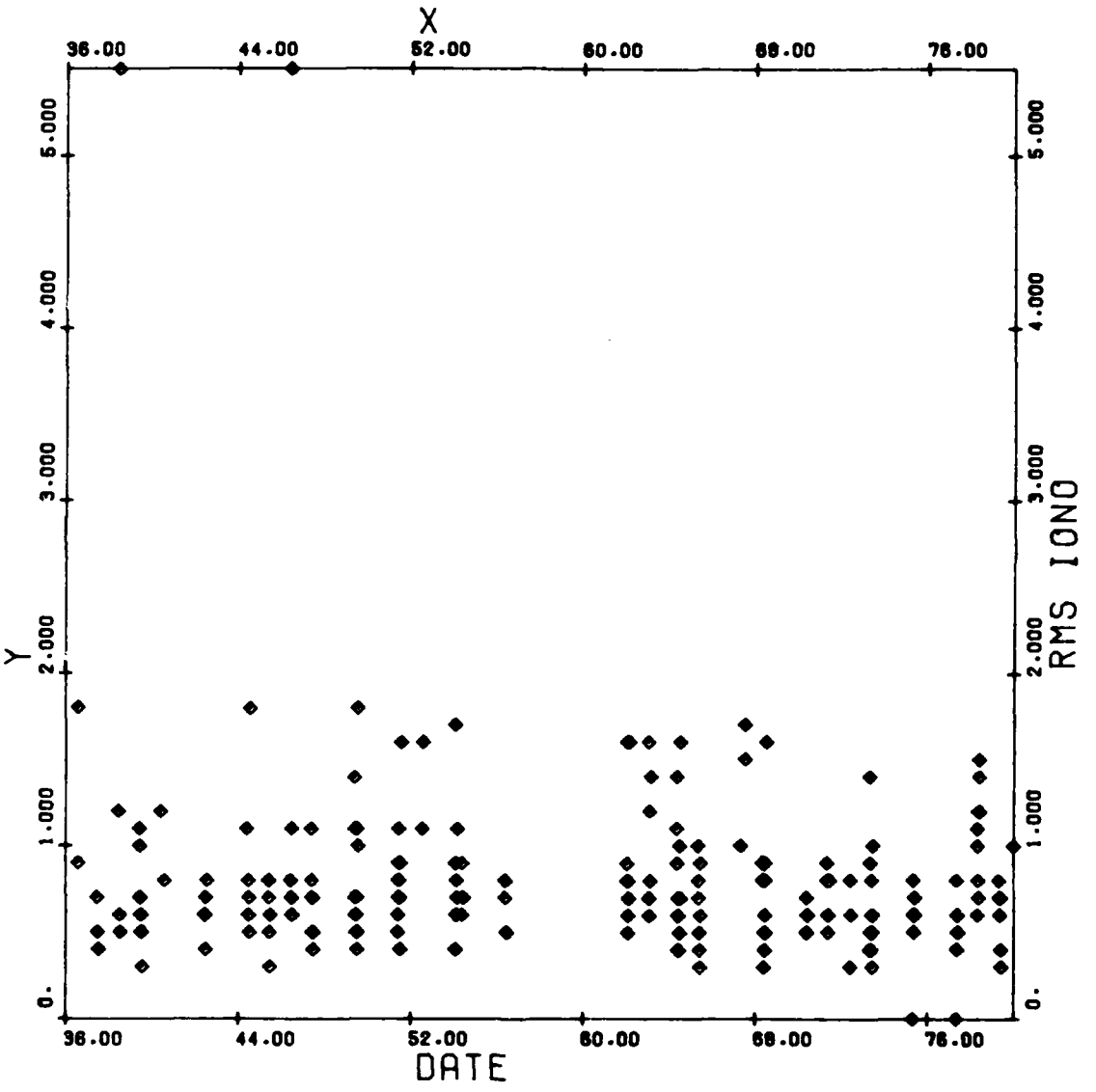

Figure 11. 20-Min Ionospheric Correction to L_1 RMS (cm) Vs Date, GPS SV-8, Yuma Proving Grounds, Days 36-80 1979

demonstration of this is available from SV7 in Figures 6 and 10. The rms of the residuals of D_u for this satellite were poor throughout the 44-day span; however, the ionospheric correction residuals in Figure 10 are unaffected and are comparable with those from any of the other satellites. This feature is certainly a plus for anyone interested in performing ionospheric measurements, because it means that they need not invest in a very low-noise, and consequently expensive, local-frequency standard.

Since the error in D_u is primarily due to $\Delta\psi$ and the error in J_u is due to ΔN, they should be independent. Therefore, the predicted error in range difference would be equal to

$$\Delta r = [(\Delta D_u)^2 + (\Delta J_u)^2]^{1/2}$$

Using the numbers derived previously, the range difference observation error should be about 4.0 cm. This is in excess of what is observed for satellites 4, 6, and 8, but less than that for satellite 7. If the primary error source is due to the random phase fluctuations of the frequency reference, then assuming that the phase fluctuations of the local reference are represented by σ_l, the estimates of the satellite values can be made using the method previously outlined. The numerical value for σ_l will be taken from the Allen variance at $T = 60$ s (Table 2). With this value fixed, a number representative of the satellite frequency reference can be calculated using the following relations:

$$\Delta D_u = \frac{\partial D_u}{\partial \psi_i} \Delta\psi_i$$

and

$$\Delta\psi_i = \{q_i^2[\eta_i(t_K + T) - \eta_i(t_K)]^2 + \varrho_i^2[\eta_l(t_K + T) - \eta_l(t_K)]^2\}^{1/2}$$

for this application

$$\Delta\psi_i = 2\pi \times 60 \times 10^6 \{(10.23 \times 154 \times \xi)^2 + (5 \times 315.07825)^2\}^{1/2} \sigma_l$$

Solution for ξ and substitution for the average ΔD_u obtained from Figures 4 through 11 over the entire 44 days gives the results listed in Table 2.

Table 2. Satellite Phase Noise Derived From Doppler Observations

SV	ΔD_u (cm)	Satellite Phase Noise $\xi\sigma_l$	Assumed Local Value σ_l
4	2.98	1.34×10^{-12}	1×10^{-12}
6	2.57	1.04×10^{-12}	1×10^{-12}
7	10.61	5.83×10^{-12}	1×10^{-12}
8	3.76	1.85×10^{-12}	1×10^{-12}

CONCLUSIONS

The formulation for converting Doppler counts into range difference observations has been developed for the case of the NGRS. The two frequency data were combined to generate the first-order ionospheric term. When this term is subtracted from the uncorrected L_1 range difference, the result is the ionospheric-corrected range difference.

The sensitivity of the observation equation to errors in the observed parameters was investigated by evaluating the partial derivatives and using them in the expression for the total derivative. Errors in the parameters were estimated and used to determine the error expected in the range difference. These estimates were then compared with examples of real observations obtained when the NGRS was on site at the Yuma Proving Ground. Agreement was reasonable and tends to confirm that the analysis is correct. Further tests are planned based upon the predictions that can be made from results developed in this report.

REFERENCES

1. *Journal of the Institute of Navigation*, Summer 1978, *25*, No. 2.
2. *Hewlett Packard Electronics Instruments and Systems*, 1980 Catalog.
3. L. R. Gibson, *Some Expansions for an Electromagnetic Wave Propagating Through a Spherically Symmetric Refracting Medium*, NSWC TR-3344 (Dahlgren, Va., June 1975).
4. H. Hendrickson, "On-Board Clock Data Processing", GPS Reference Ephemeris Data Analysis Working Group Presentation, 14 November 1979.

APPENDIX A

Frequency Spectrum of the *P* Code Modulation

Define the phase argument of a cosine function to be $\theta(t)$ where

$$\theta(t) = \omega_c t + \theta_0 + kg(t)$$

The parameters ω_c, θ_0, and k are constants, and $g(t)$ is a random gate function of unit amplitude. The random character of $g(t)$ is best demonstrated by Figure A-1. A mathematical expression for $g(t)$ can be devised by the time translation of an elementary gate function centered on zero as in Figure A-2. Using this concept, we can express the random gate function as the sum of translated $g'(t)$'s multiplied by a random variable a_l.

$$g(t) = \sum_{l=-n}^{n} a_l g'(t - l\tau) \tag{A-1}$$

The value of a_l is either one or zero depending upon the outcome of some random process related to the subscript l.

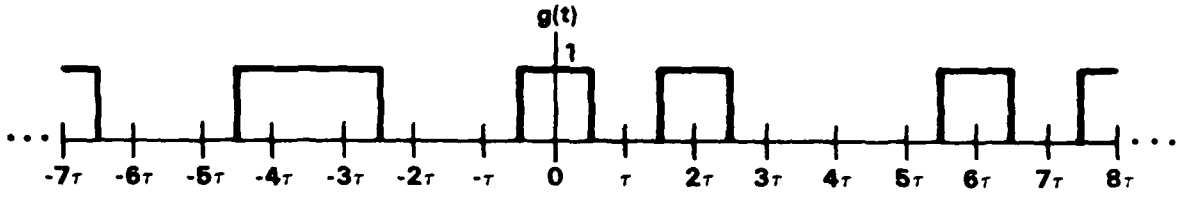

Figure A-1. Random Gate Function

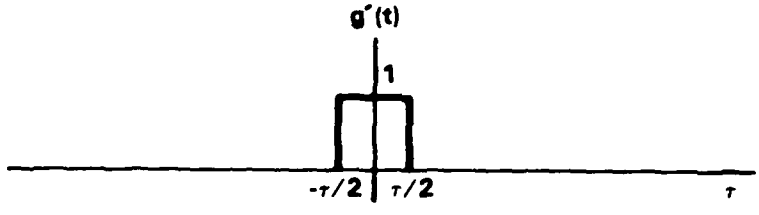

Figure A-2. Elementary Gate Function Centered On Zero

If we choose $\theta_0 = 0$ and $k = \pi$, then $\theta(t)$ becomes

$$\theta(t) = \omega_c t + \pi g(t) \tag{A-2}$$

Now according to the definition of $g(t)$, the value of $\theta(t)$ can be only $\omega_c t + \pi$ or $\omega_c t$. This is the *biphase* part of the argument. When $\theta(t)$ is introduced into a cosine function, the result is

$$\cos \theta(t) = \cos[\omega_c t + \pi g(t)]$$

which when expanded becomes

$$\cos \theta(t) = \cos \omega_c t \cos \pi g(t) - \sin \omega_c t \sin \pi g(t)$$

Now, since $\pi g(t)$ is either 0 or π, the second term vanishes, which leaves just

$$\cos \theta(t) = \cos \omega_c t \cos \pi g(t) \tag{A-3}$$

The second cosine factor here is either +1 or -1 depending on whether the argument is 0 or π, which in turn depends upon whether a_i is 1 or 0. Since this is the case, we can construct a new factor to replace

$$\cos \pi g(t)$$

which behaves in the same manner. Let this be $m(t)$ where

$$m(t) = 2g(t) - 1.$$

Equation A-3 written using this new factor is

$$\cos \theta(t) = [2g(t) - 1] \cos \omega_c t. \tag{A-4}$$

The random function $m(t)$ represents the pseudo-random code modulating $\cos \omega_c t$. The Fourier transform of the elementary gate function is

$$F\{g'(t)\} = \tau \frac{\sin \omega\tau/2}{\omega\tau/2} \equiv G(\omega) \tag{A-5}$$

Employing the time shift property,

$$F\{h(t - T)\} = H(\omega)\, e^{-j\omega T}$$

allows $F\{g'(t - n\tau)\}$ to be evaluated from $F\{g'(t)\}$ as shown below:

$$F\{g'(t - n\tau)\} = \tau \frac{\sin \omega\tau/2}{\omega\tau/2} e^{-j\omega n\tau} = G(\omega)\, e^{-j\omega n\tau}$$

It follows then that

$$F\{g(t)\} = \tau \frac{\sin \omega\tau/2}{\omega\tau/2} \sum_{i=-n}^{n} a_i e^{-j\omega i\tau} = G(\omega) \sum_{i=-n}^{n} a_i e^{-j\omega i\tau} \tag{A-6}$$

with the implication that the contribution from any term of the sum with $a_i = 0$ is also zero. Thus, the frequency spectrum of $g(t)$ is a summation of the form shown above with an arbitrary number of possible contributors missing. The terms missing are specified by the outcome of the random process controlling a_i.

The basic frequency spectrum (Equation A-5) behaves as a sin x/x function multiplied by a series of complex function given by the summation in Equation A-6. The first nulls of $G(\omega)$ are when

$$\frac{2\pi f_0 \tau}{2} = \pi,$$

This frequency is 10.23 MHz for the GPS *P* code. Thus, the bandwidth between first nulls is 20.46 MHz and contains the majority of the transmitted energy. Since energy per unit bandwidth is proportional to $|G(\omega)|^2$, a comparison can be made by integrating $|G(\omega)|^2$ between zero and infinity and again between zero and the first null.*

$$\int_0^{\pi} \frac{\sin^2 x \, dx}{x^2} = \frac{\pi}{2} = 1.57079$$

whereas

$$\int_0^{\infty} \frac{\sin^2 x \, dx}{x^2} = 1.41815$$

This ratio shows that the fraction of energy between first nulls is 90 percent of the total.

It is interesting to see how the gate function pictured in Figure A-2 changes when $G(\omega)$ is cut off due to the finite bandwidth of the transmission and receiving systems. We can approximate this effect by defining a gate function in the frequency domain $W(\omega)$ such that it is unity between $\pm \omega_c$ and zero elsewhere. This function (pictured in Figure A-3) is then multiplied by $G(\omega)$, which gives the product $G(\omega)\ W(\omega)$. Since multiplication in one domain is equivalent to convolution in the other domain, the resulting function in the time domain is the pulse

$$p(t) = \int_{-\infty}^{\infty} w(t - \xi)\, g(\xi)\, d\xi$$

Since

$$w(t) = \frac{\omega_c}{2\pi} \frac{\sin \omega_c t / 2}{\omega_c t / 2} \qquad \text{(Figure A-4)}$$

and $g(t)$ is as before, zero for $|t| > \tau/2$ (Figure A-5), the convolution integral is

$$p(t) = \int_{-\infty}^{\infty} \frac{\omega_c}{2\pi} \frac{\sin \omega_c [2(t - \xi)]}{\omega_c [2(t - \xi)]} g(\xi)\, d\xi$$

*B. P. Lathi, *Signals, Systems, and Communication*, John Wiley and Sons, p. 150.

or

$$p(t) = \frac{\omega_s}{2\pi} \int_{t-\tau/2}^{t+\tau/2} \frac{\sin \omega_s/2(t-\xi)}{\omega_s/2(t-\xi)}\, d\xi$$

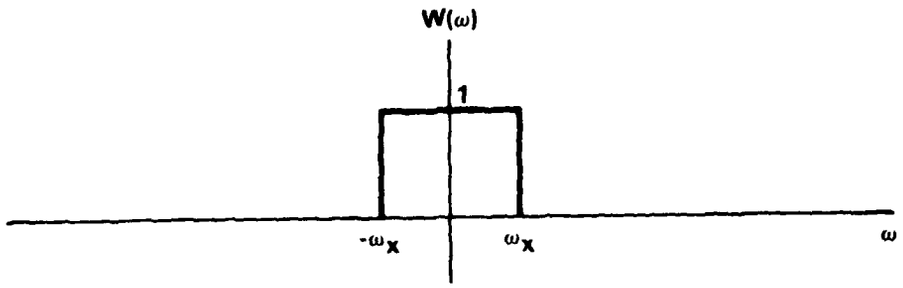

Figure A-3. Elementary Gate Function Centered On Zero Frequency

This bandwidth limiting causes appreciable distortion in the original pulse shape (Figure A-6); however, this does not appear to degrade the resulting pseudo-range measurement to any great degree. The GPS receiver cross-correlates the received pulses or chips with a locally generated code. The result of the cross-correlation of one local chip with the received bandlimited chip is shown in Figure A-7. This correlation curve is then advanced one-half chip, $\tau/2$, and retarded one-half chip. The retarded chip is then subtracted from the advanced chip defining a zero crossing, which indicates the exact time of maximum correlation. The result of these manipulations is shown in Figure A-8. This is a much more sensitive method of obtaining maximum correlation because the actual correlation curve (Figure A-7) has a rounded top, whereas the advanced minus retarded curve has a well-defined zero crossing due to the steep slope. This method of finding maximum correlation is called a delay lock loop.*

If there were no bandwidth limiting, the chip shown in Figure A-5 would be received with perfect fidelity. Consequently, the cross-correlation function would have a triangular shape (Figure A-9) instead of the smooth curve of Figure A-7. The shape of the curve from Figure A-9 corresponding to that of Figure A-8 is drawn as Figure A-10. These two curves are more closely approximated if the bandwidth of the receiver is increased. This result is illustrated in Figures A-11 through A-14 for the case where $\omega_s = 2\pi/\tau$, and in Figures A-15 through A-18 the case where $\omega_s = 3\pi/\tau$.

*R. C. Dixon, *Spread Spectrum Systems*, John Wiley and Sons, p. 205.

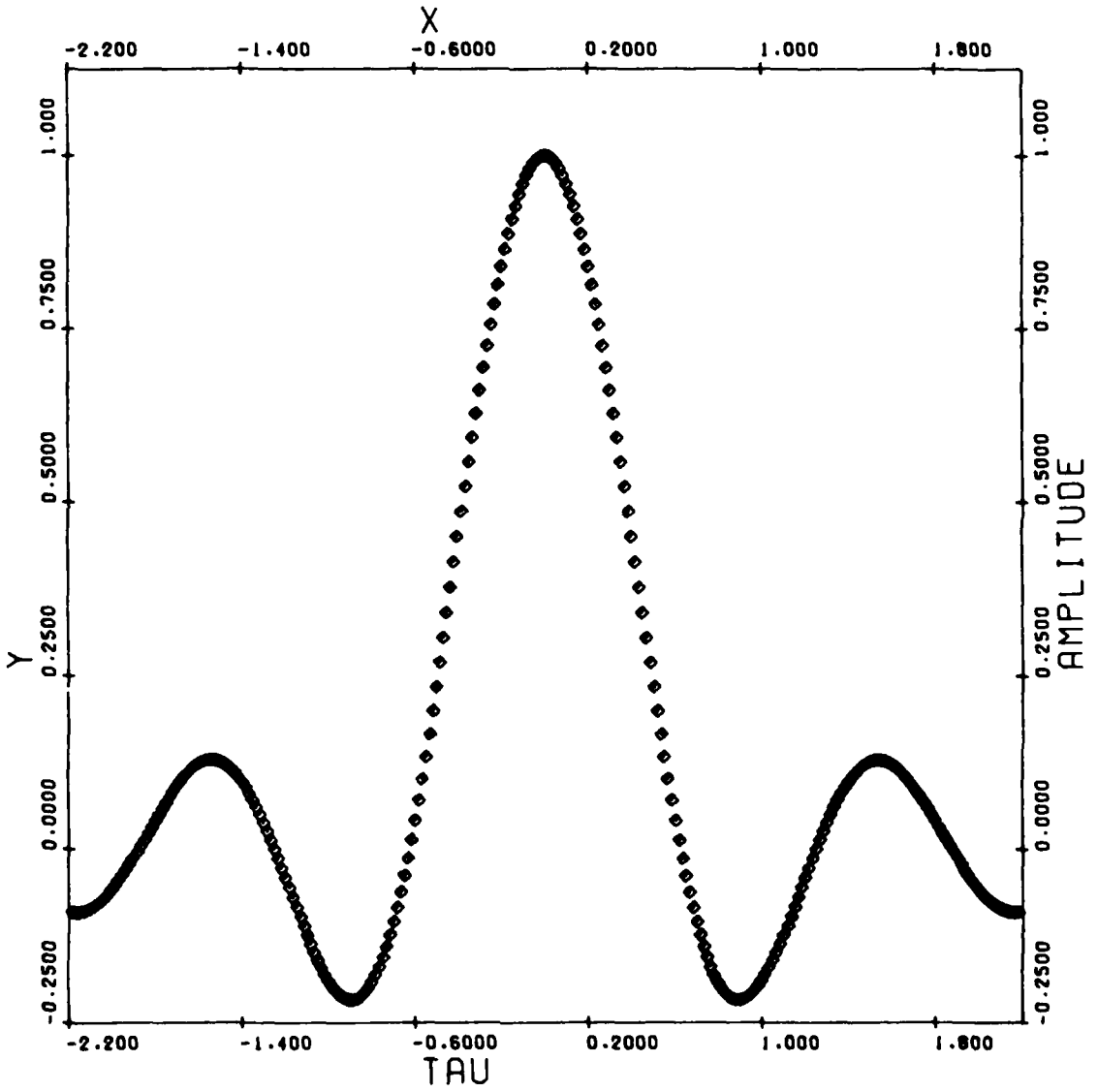

Figure A-4. Frequency Domain Gate Function Transformed to the Time Domain, ω_o = PI/TAU

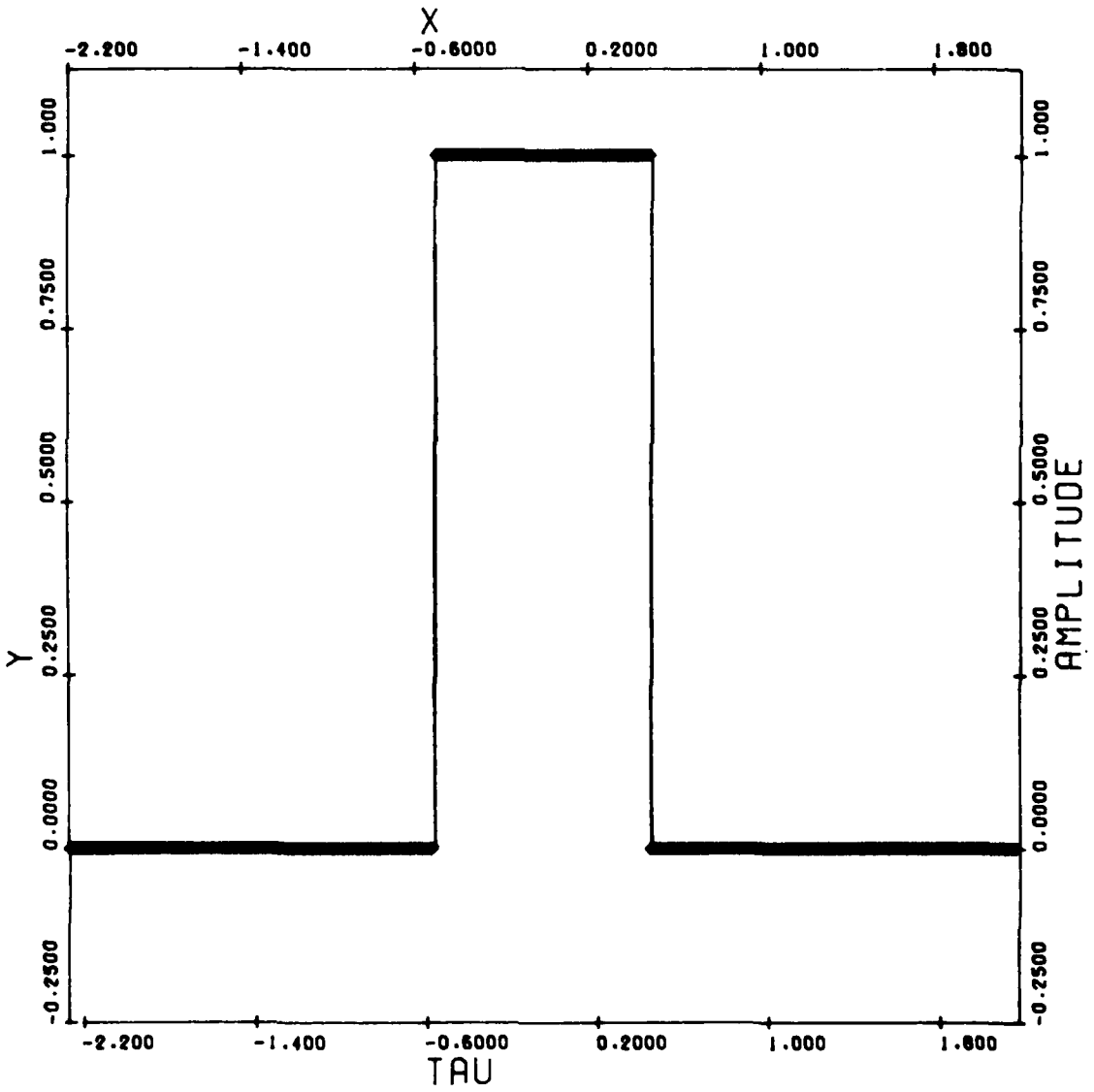

Figure A-5. Elementary Gate Function in Time Domain, TAU = 97.752 ns

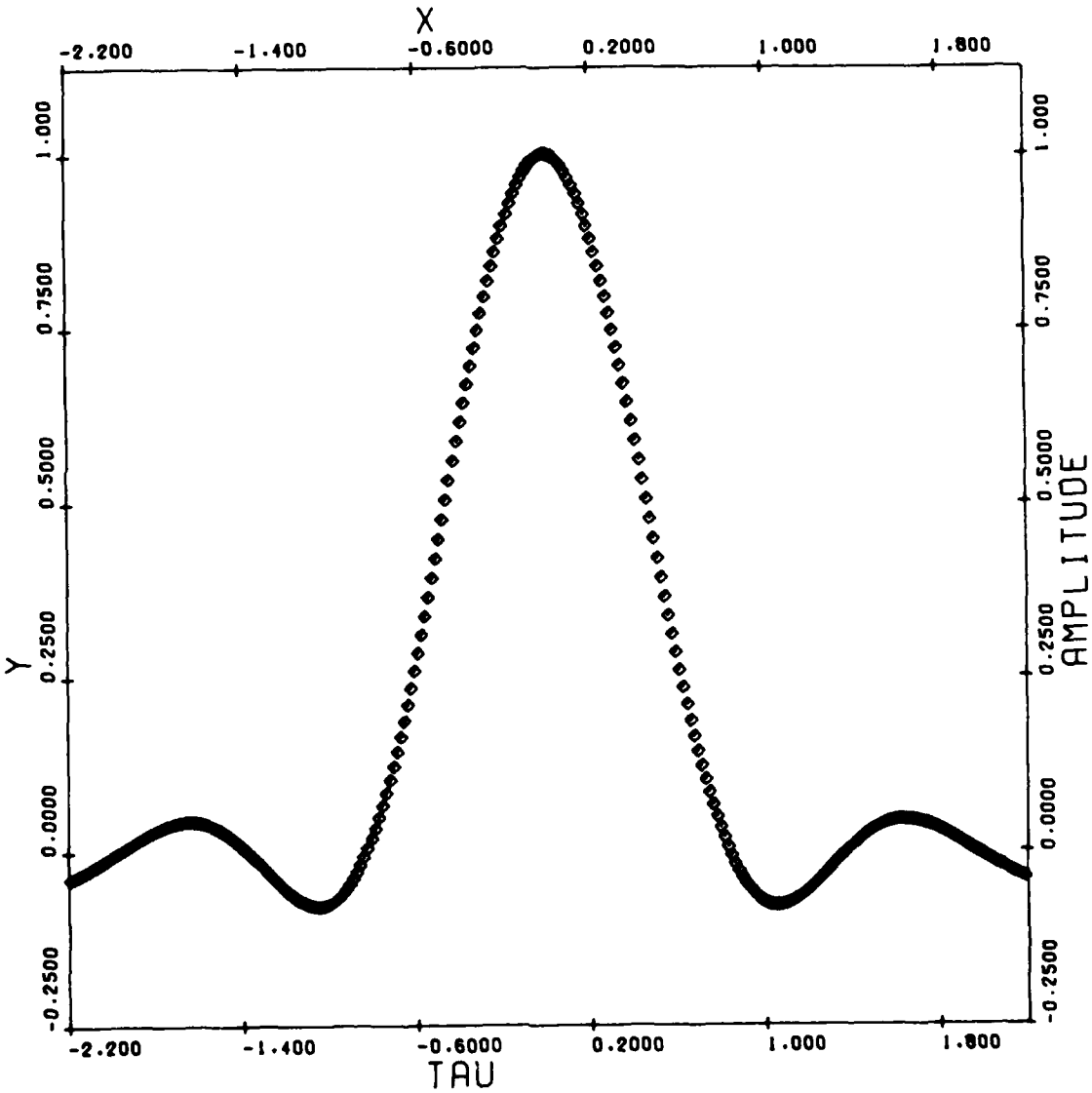

Figure A-6. Convolution of Elementary Gate With Transformed Gate, ω_0 = PI/TAU
(Pulse Shape of Received Chips Due to Finite Bandwidth)

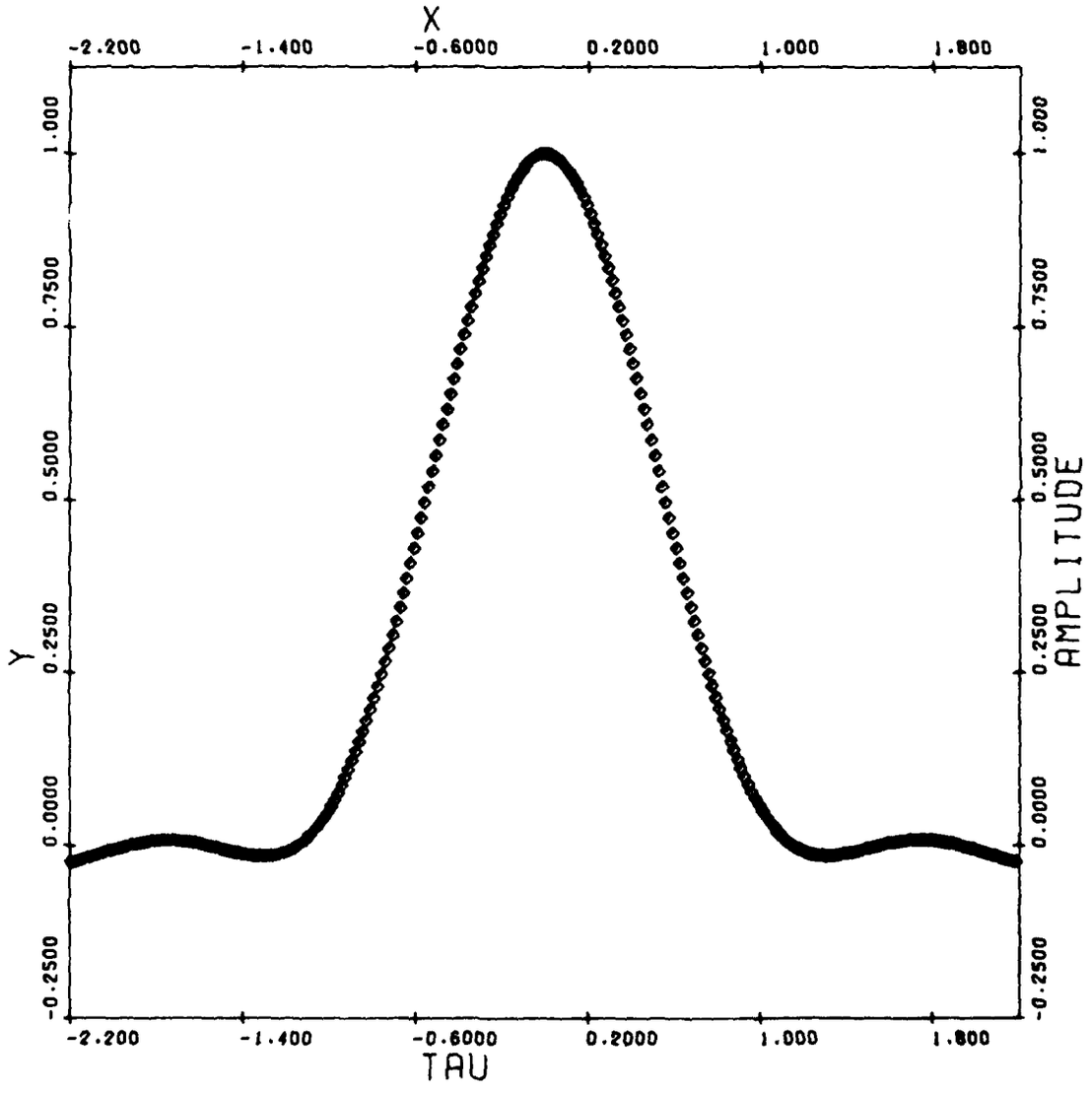

Figure A-7. Cross Correlation of Received Chip With Locally Generated Chip, ω_0 = PI/TAU

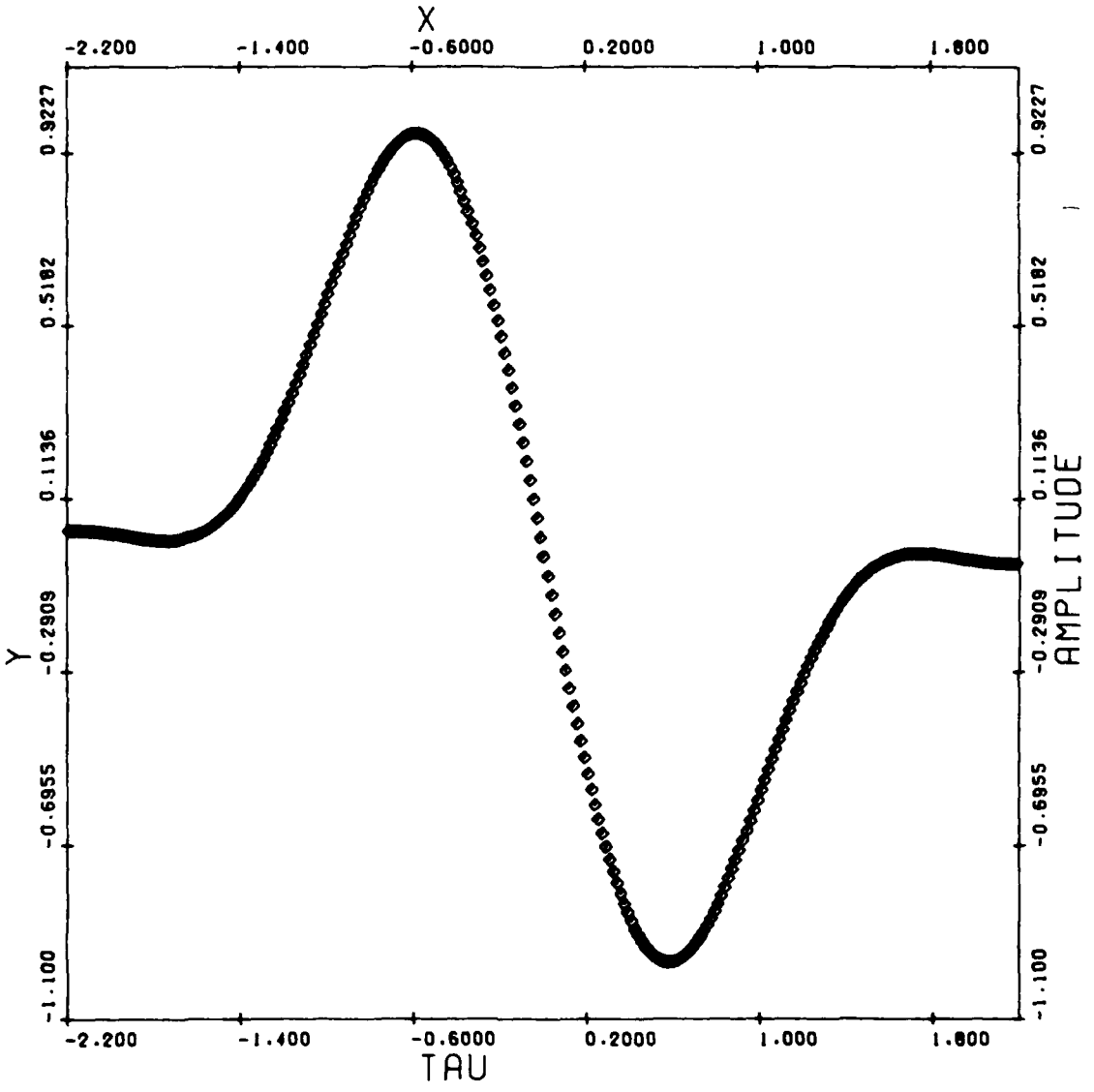

Figure A-8. Half Chip Early Minus Half Chip Late Correlation Curve, ω_n = PI/TAU

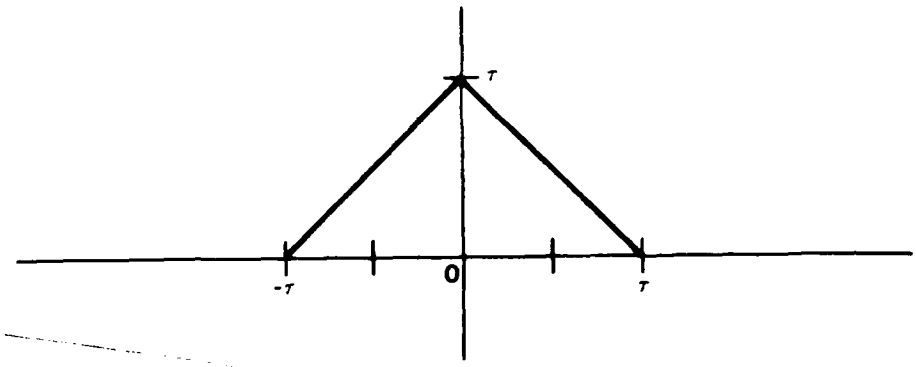

Figure A-9. Cross Correlation Function of Two Gate Functions of Width τ

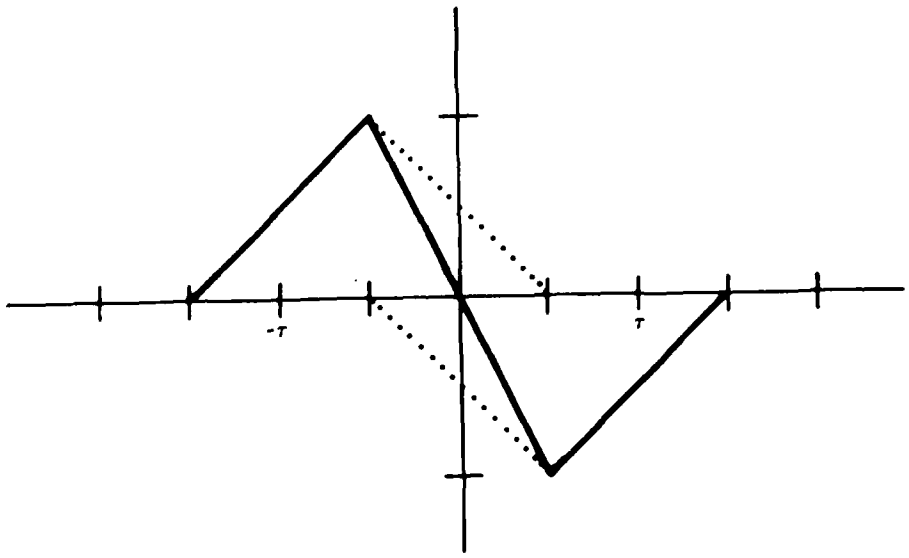

Figure A-10. Half Chip Early Minus Half Chip Late Correlation Curve

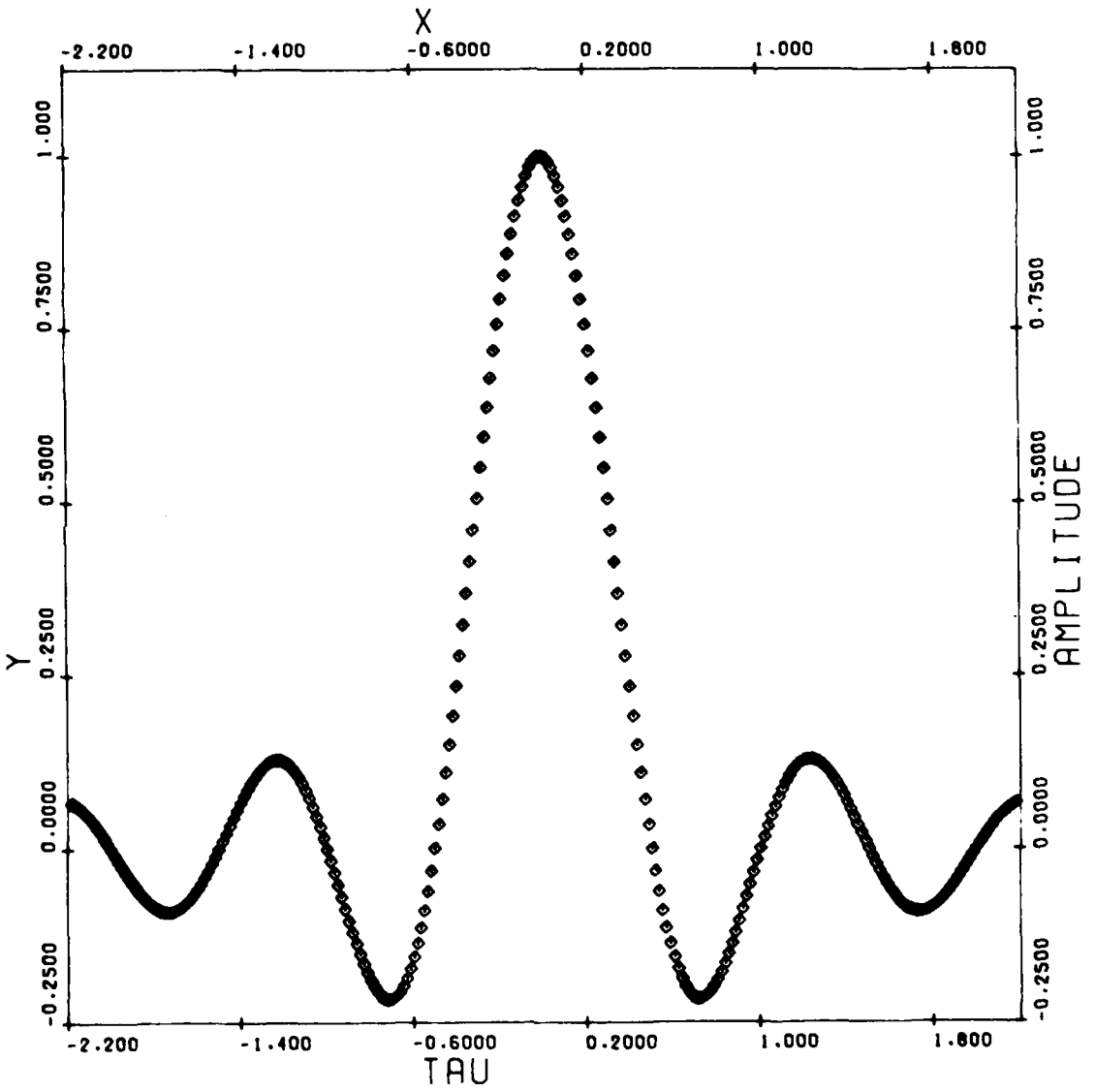

Figure A-11. Frequency Domain Gate Function Transformed to the Time Domain, ψ_e = 2 PI/TAU

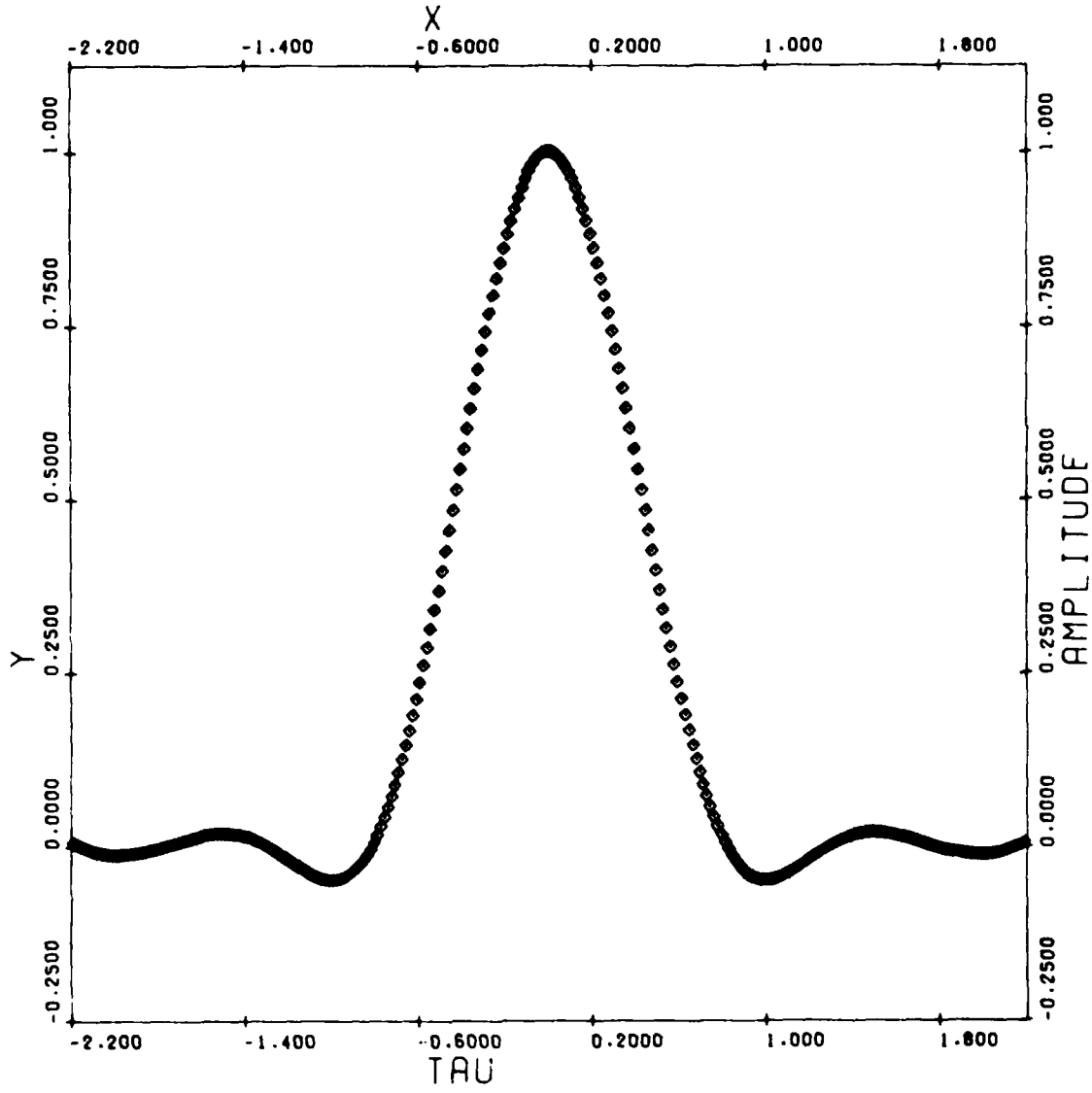

Figure A-12. Convolution of Elementary Gate With Transformed Gate, ω_0 = 2 PI/TAU (Pulse Shape of Received Chips Due to Finite Bandwidth)

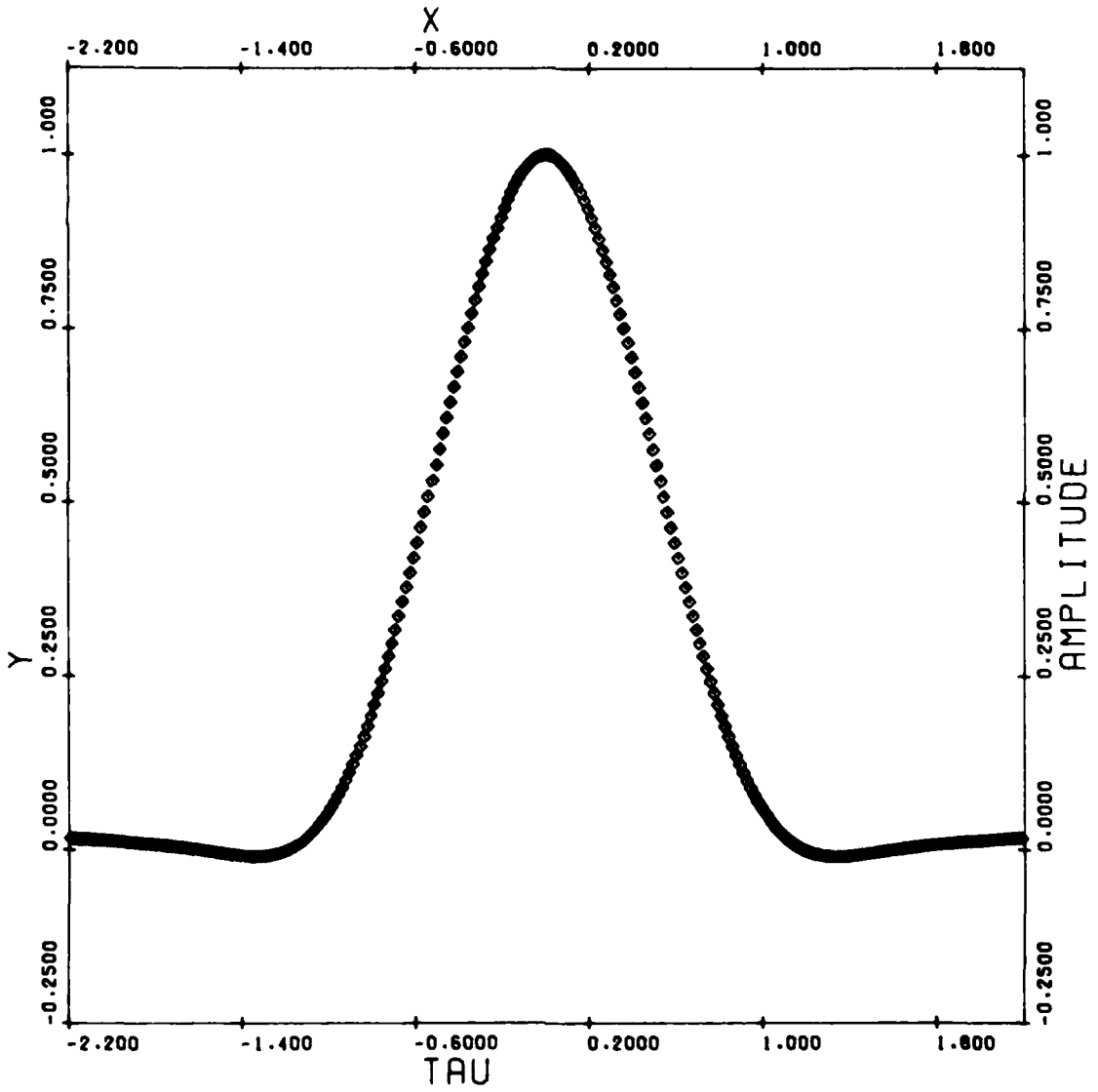

Figure A-13. Cross Correlation of Received Chip With Locally Generated Chip, ω_0 = 2 PI/TAU

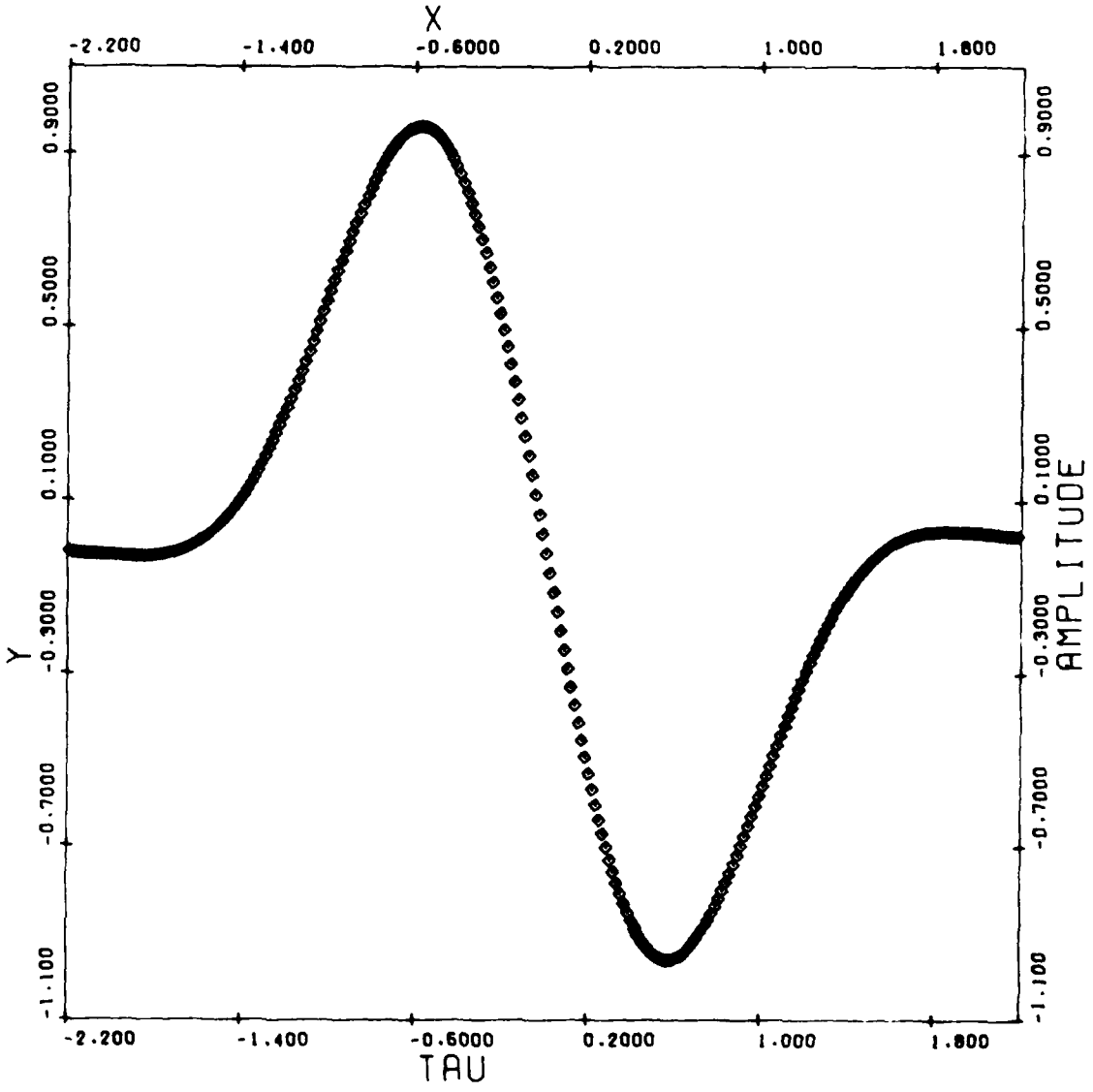

Figure A-14. Half Chip Early Minus Half Chip Late Correlation Curve.
ω_0 = 2 PI/TAU

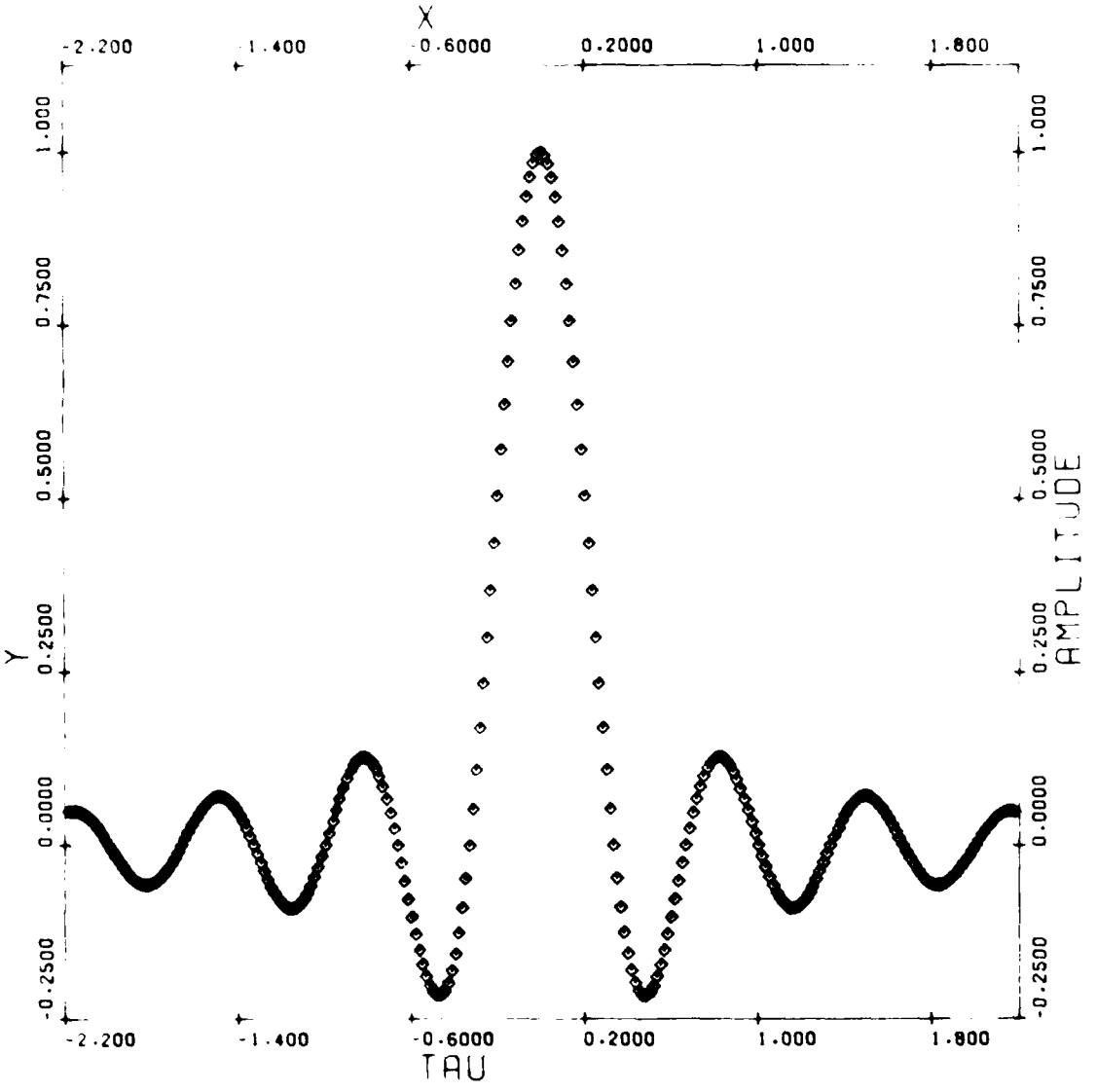

Figure A-15. Frequency Domain Gate Function Transformed to the Time Domain, [illegible] 3 PI TAU

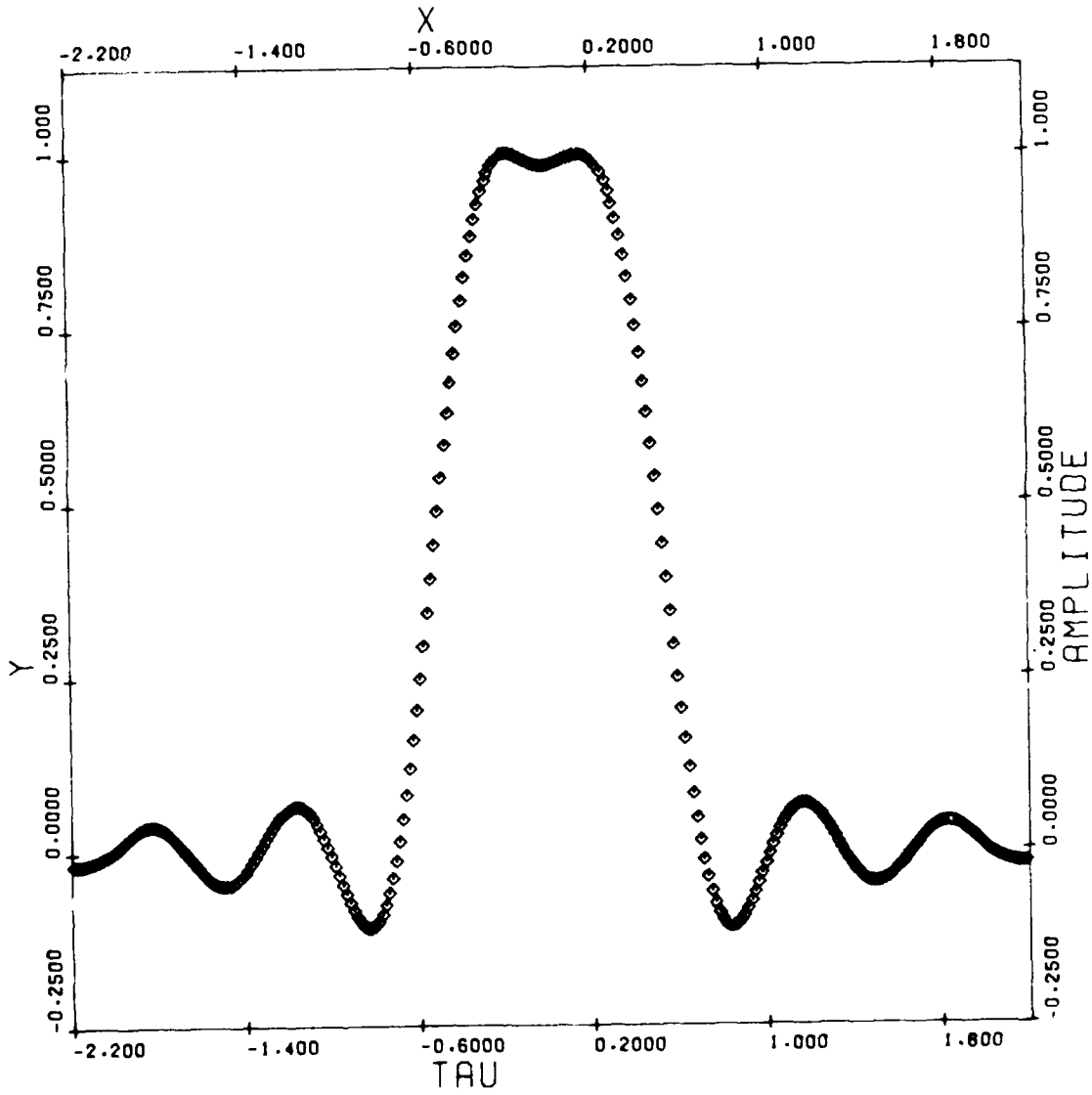

Figure A—16. Convolution of Elementary Gate With Transformed Gate, ω_0 = 3 PI/TAU
(Pulse Shape of Received Chips Due to Finite Bandwidth)

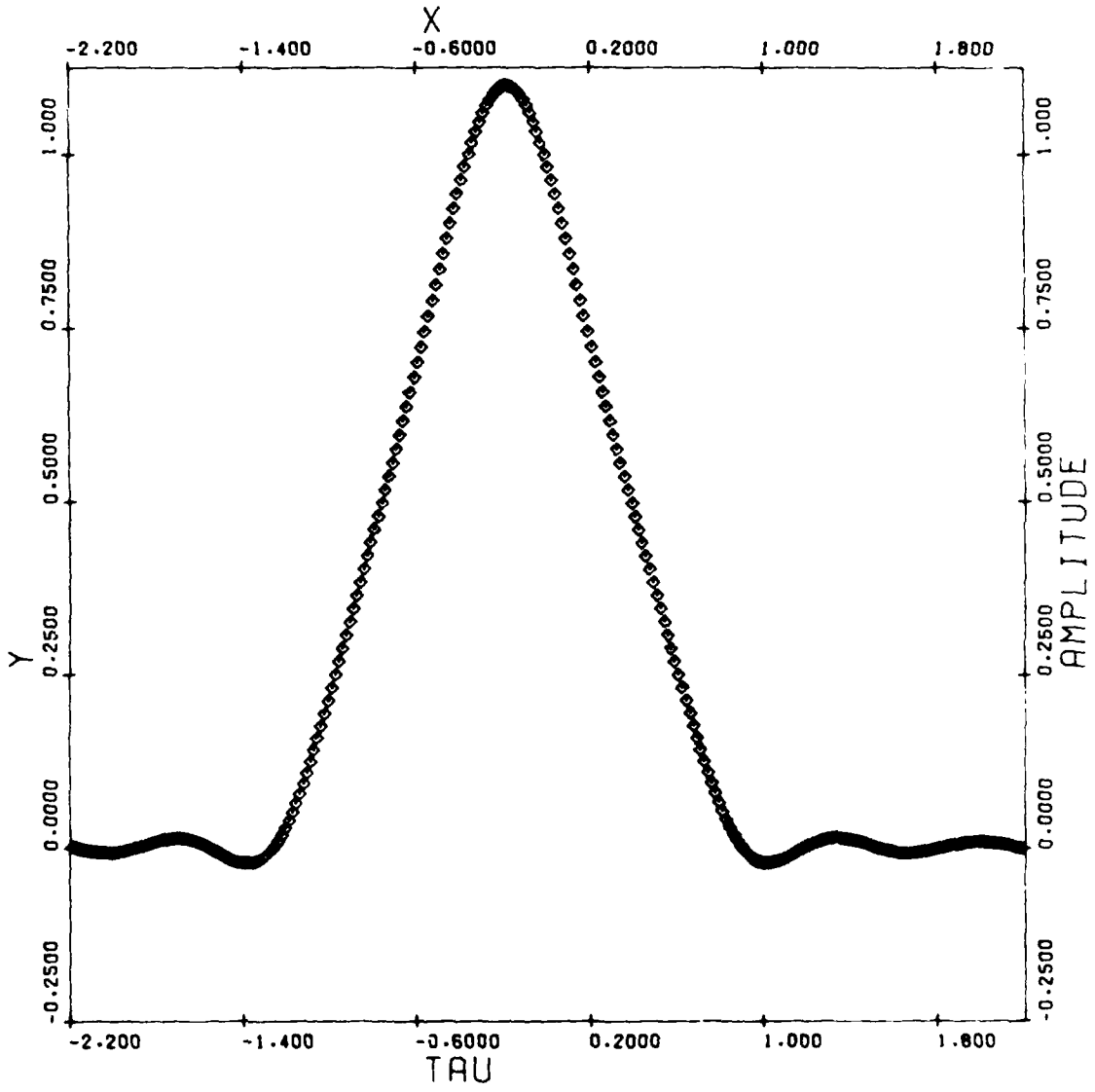

Figure A-17. Cross Correlation of Received Chip With Locally Generated Chip, $\omega_0 = 3$ PI/TAU

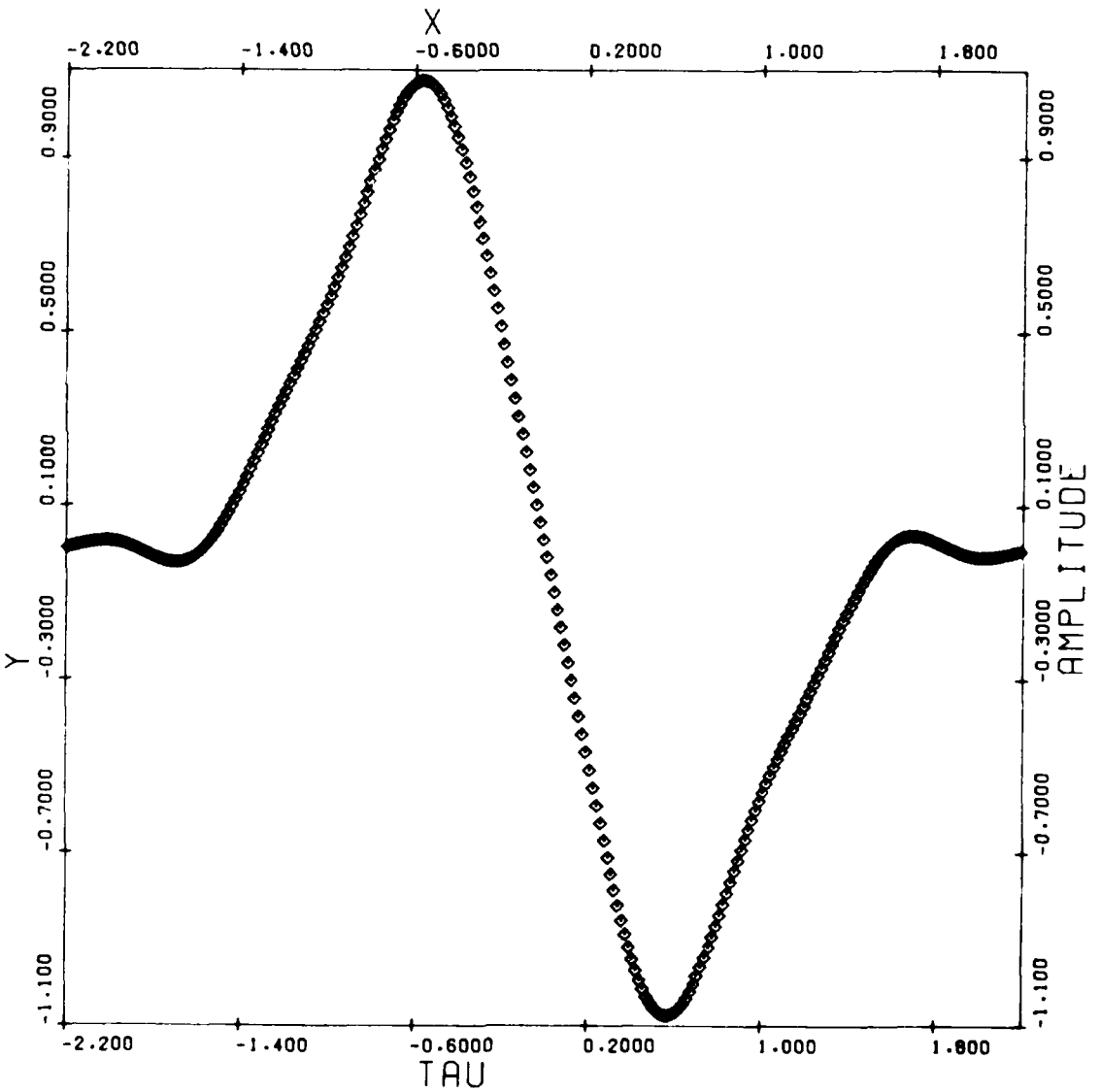

Figure A-18. Half Chip Early Minus Half Chip Late Correlation Curve, ω_0 = PI/TAU

APPENDIX B

LOCAL CLOCK CORRECTION FROM PSEUDO-RANGE MEASUREMENT

The single-frequency pseudo-range is used to obtain the local clock correction. As was illustrated in Figure 2 of the text, this correction, τ_f, can be obtained if τ_s (the satellite offset from GPS) and τ_0 (the satellite offset from the local clock) are known. The predicted values for τ_s can be obtained by decoding the satellite navigation message.* The corresponding value for τ_0 can be found if the true slant range to the satellite is known at the time of each observation. A reference trajectory, or the data from the navigation message, can be used to determine the satellite position. At the time transmission, let this be $\bar{r}_s(t_1)$. The receiver position in inertial space at the time of reception is $\bar{r}_R(t_2)$. The slant range $\bar{r}$ is the difference

$$\bar{r}(t_2) = \bar{r}_s(t_1) - \bar{r}_R(t_2)$$

Therefore, the propagation time is $\tau_r = r/c$. Propagation delays due to refraction are not included in this calculation, since the errors they contribute are less than the 1-μs accuracy desired.

The pseudo-range measurement is concluded at t_2 when the satellite epoch is received. Consequently, the local offset will be time tagged t_2, which equals the satellite epoch of transmission t_1 plus the correction to the satellite clock τ_s plus the propagation delay τ_r. Therefore, the local offset is

$$\tau_0(t_2) \equiv \tau_0(t_1 + \tau_s + \tau_r) = \tau_\rho - \tau_r$$

From Figure 2, the correction to the local epoch τ_f must be

$$\tau_f = \tau_s - \tau_0 = \tau_s - \tau_\rho + \tau_r$$

where τ_s is obtained from the satellite NAVDATA message and is calculated using the station and satellite positions at the times of reception and transmission, respectively. The pseudo-range observation is τ_ρ.

The data τ_f and its time argument t_2 can be collected and fitted by a polynomial whose coefficients were obtained using least squares. The polynomial would have the form

$$\tau_f(t) = \sum_{k=0}^{n} a_k t^k$$

Using this, the local time is corrected by putting the apparent local time in for t and calculating the correction $\tau_f(t)$. Several iterations may be used to improve the accuracy.

*Van Dierendonck, Russell, Kopitzke, Birnbaum, "The GPS Navigation Message", *Navigation*, Vol. 25, No. 2, Summer 1978.

APPENDIX C

MAXIMUM DOPPLER AND DOPPLER RATE

This simplified development establishes a worst case configuration for relative satellite-earth station motion. It is useful in that it sets limits on the maximum expected Doppler frequency (velocity) and Doppler rate (acceleration).

The worst case is presumed to be a satellite at GPS altitude in a retrograde equatorial orbit (Figure C-1). No GPS satellite is ever expected to be in such an orbit, so the results calculated here will determine an upper limit on the velocity and accelerations along the slant range vector.

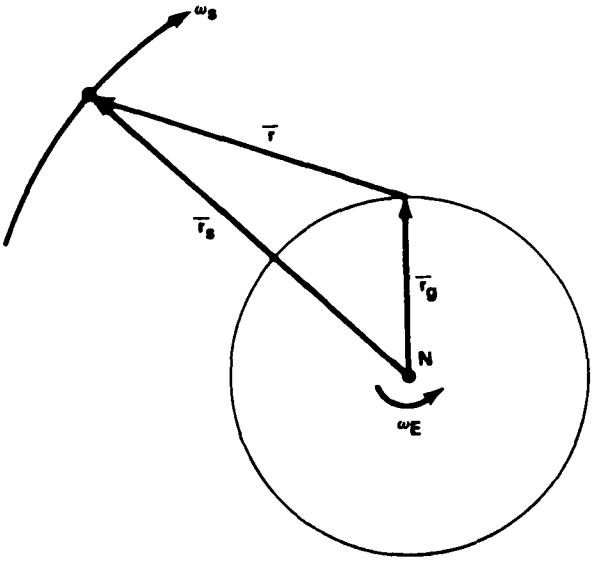

Figure C-1. Retrograde Equatorial Orbit Geometry

From the law of cosines

$$r^2 = r_e^2 + r_s^2 - 2r_e r_s \cos\theta \qquad \text{(C-1)}$$

Then

$$2r\,\frac{dr}{dt} = 2r_e r_s \sin\theta\,\frac{d\theta}{dt} \qquad \text{(C-2)}$$

Assume that ω_e and ω_r are constant.

$$\frac{d\theta}{dt} = \omega = \omega_e + \omega_r$$

$$\frac{dr}{dt} = v = r_s r_e r^{-1} \omega \sin\theta \tag{C-3}$$

$$\frac{dv}{dt} = r_s r_e \omega \left[r^{-1} \cos\theta \frac{d\theta}{dt} - \sin\theta r^{-2} \frac{dr}{dt} \right] \tag{C-4}$$

Set $dv/dt = 0$ to find the θ, which gives the maximum velocity:

$$r^2 \cos\theta = r_s r_e \sin^2\theta$$

This can be rewritten by substituting for r^2:

$$\frac{r_s^2 + r_e^2}{r_s r_e} \cos\theta = 1 + \cos^2\theta \tag{C-5}$$

This result is independent of ω. Substituting $r_s = 26560$ km, $r_e = 6378$ km results in a value for $\theta \cong 76°$. The combined angular velocity

$$\omega = \frac{2\pi}{86164} + \frac{4\pi}{86164} = \frac{6\pi}{86164}$$

Evaluating Equation C-3 at $\theta = 76°$ gives the maximum velocity

$$v_{max} = \frac{r_s r_e \omega \sin\theta}{[r_s^2 + r_e^2 - 2r_s r_e \cos\theta]^{1/2}} = 1395 \text{ m/s} \tag{C-6}$$

At the two frequencies, $L_1 = 1575.42$ MHz and $L_2 = 1227.6$ MHz, the Doppler shift is approximately 7326 Hz on L_1 and 5708 Hz on L_2. The acceleration is obtained by substituting Equation C-3 into Equation C-4:

$$\frac{dv}{dt} = r_s r_e \omega [r^{-1}\omega \cos\theta - \sin^2\theta r^{-3} r_s r_e \omega]$$

$$\frac{dv}{dt} = r_s r_e \omega^2 r^{-1} [\cos\theta - r^{-2} r_s r_e \sin^2\theta]$$

By inspection, it is evident that dv/dt will be greatest when $\theta = 0$. The second term in brackets is zero when $\theta = 0$ and is greater than zero for any other θ. Also, Figure C-1 shows that r will be a minimum at $\theta = 0$, which makes r^{-1} and, consequently, dv/dt a maximum. At $\theta = 0$, Equation C-4 becomes

$$\left.\frac{dv}{dt}\right|_{\theta=0} = \frac{r_s r_e \omega^2}{[r_s^2 + r_e^2 - 2r_s r_e]^{1/2}} = 0.402 \text{ m/s}^2$$

The maximum Doppler rate is also at the angle of maximum acceleration. At the two GPS frequencies, these are 2.1 Hz/s on L_1 and 1.6 Hz/s on L_2.

The error in the Doppler count over 1 min due to the use of the average frequency can be estimated using these rates. With an L_1 rate of 2.1 Hz/s, the average frequency can be in error by about 63 Hz at each end of the 60-s count interval. Assuming a value for the fractional interval equal to a full cycle (using the zero Doppler frequency 28750 Hz), the count will be in error by 63/28,750 = 0.002. This is equivalent to a 0.04-cm error in the delta range measurement at L_1. The corresponding error at L_2 is 0.03 cm.

DISTRIBUTION

Shell Resources Canada Ltd.
400 4th Ave. S.W.
Calgary, Alberta
Canada T2P0J4
ATTN: Alex Hittel (4)

TASC
6 Jacob Way
Reading, MA 01867
ATTN: Gary Matchett

Charles R. Payne
6592/SPO, Code YED
P.O. Box 92960
World Wav Postal Center
Los Angles, CA 90009

AFGL - PHP
Hanscom AFB
Bedford, MA 01731
ATTN: Jack Klobuchar

STI
1195 Bordeaux Drive
Sunnyvale, CA 94086
ATTN: J. J. Spilker, Jr. (5)

IBM
18100 Frederick Pike
Gaithersburg, MD 20760
ATTN: Fritz Byrne (3)

Applied Physics Laboratory
Johns Hopkins University
Johns Hopkins Road
Laurel, MD 20810
ATTN: Reginald Rhue
Joseph Wall
Edward Prozeller

Defense Mapping Agency Headquarters
U.S. Naval Observatory
Building 56
Washington, DC 20305
ATTN: Dr. Charles Martin (STT)

DISTRIBUTION (Continued)

Defense Mapping Agency
Aerospace Center
2nd & Arsenal St.
St. Louis, MO 63118
ATTN: George Stentz

Professor Charles Counselman, III
54-620 Massachusetts Institute of Technology
77 Massachusetts Ave.
Cambridge, MA 02139

Dr. Peter Bender
Joint Institute for Laboratory Astrophysics
University of Colorado
Boulder, CO 80302

Magnavox Research Laboratory
2829 Moricopa St.
Torrance, CA 90503
ATTN: Mr. Tom Starsel

CAPT John Bossler
6001 Executive Blvd.
Rockville, MD 20852
ATTN: OA/C1X8

Mr. Clyde Goad
6001 Executive Blvd.
Rockville, MD 20852
ATTN: OA/C1X8

Defense Mapping Agency
Hydrographic/Topographic Center
Code GST
6500 Brookes Lane
Washington, DC 20315
ATTN: Ben Roth
Hank Heuerman
Fran Varnum

U.S. Geological Survey
526 National Center
12201 Sunrise Valley Drive
Reston, VA 22092
ATTN; COL Paul E. Needham

DISTRIBUTION (Continued)

Defense Technical Information Center
Cameron Station
Alexandria, VA 22314 (12)

Library of Congress
Washington, DC 20540
ATTN: Gift and Exchange Division (4)

Local:

E31 (GIDEP)
E41
F14 (Saffos)
K10 (8)
K13 (Hermann)
X210 (20)
(6)


DATE
ILME